

Dissertations and Theses

5-2017

Battery Centric Serial Hybrid Aircraft Performance and Design Space

Lenny Gartenberg

Follow this and additional works at: <https://commons.erau.edu/edt>

 Part of the [Aerospace Engineering Commons](#)

Scholarly Commons Citation

Gartenberg, Lenny, "Battery Centric Serial Hybrid Aircraft Performance and Design Space" (2017).
Dissertations and Theses. 327.
<https://commons.erau.edu/edt/327>

This Thesis - Open Access is brought to you for free and open access by Scholarly Commons. It has been accepted for inclusion in Dissertations and Theses by an authorized administrator of Scholarly Commons. For more information, please contact commons@erau.edu.

BATTERY CENTRIC SERIAL HYBRID AIRCRAFT PERFORMANCE AND
DESIGN SPACE

A Thesis

Submitted to the Faculty

of

Embry-Riddle Aeronautical University

by

Lenny Gartenberg

In Partial Fulfillment of the

Requirements for the Degree

of

Master of Science in Aerospace Engineering

May 2017

Embry-Riddle Aeronautical University

Daytona Beach, Florida

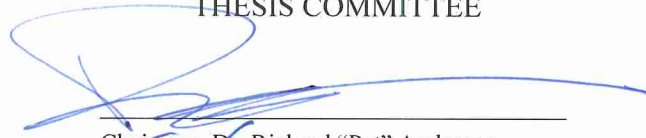
BATTERY CENTRIC SERIAL HYBRID AIRCRAFT PERFORMANCE AND
DESIGN SPACE

by

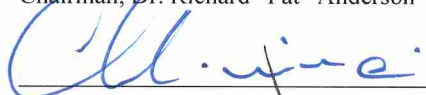
Lenny Gartenberg

A Thesis prepared under the direction of the candidate's committee chairman, Dr. Richard "Pat" Anderson, Department of Aerospace Engineering, and has been approved by the members of the thesis committee. It was submitted to the School of Graduate Studies and Research and was accepted in partial fulfillment of the requirements for the degree of Master of Science in Aerospace Engineering.

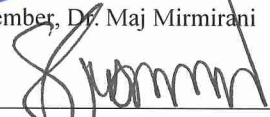
THESIS COMMITTEE



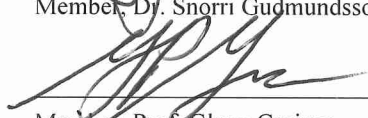
Chairman, Dr. Richard "Pat" Anderson



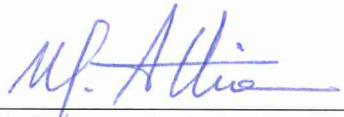
Member, Dr. Maj Mirmirani



Member, Dr. Snorri Gudmundsson



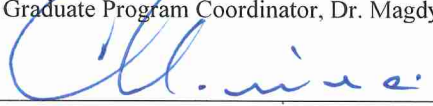
Member, Prof. Glenn Greiner



Department Chair, Dr. Anastasios Lyrintzis
or Graduate Program Coordinator, Dr. Magdy Attia

Date

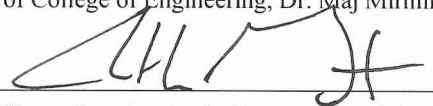
4.11.2017



Dean of College of Engineering, Dr. Maj Mirmirani

Date

4/10/17



Vice Chancellor, Academic Support, Dr. Christopher Grant

Date

4/11/17

TABLE OF CONTENTS

LIST OF TABLES	v
LIST OF FIGURES	vi
SYMBOLS.....	viii
ABBREVIATIONS	x
ABSTRACT.....	xi
1. Introduction.....	1
1.1. Motivation	1
1.2. Problem Statement	4
1.3. Objectives	5
1.3.1. General Objective.....	5
1.3.2. Specific Objectives	5
2. Literature Review	7
2.1. Alternative Propulsion.....	7
2.2. Serial Hybrid	11
2.3. Batteries	13
2.4. Electric Motors	16
2.5. Propeller Theory	20
2.6. Aircraft Efficiency.....	22
2.7. Aircraft Noise	24
3. Methodology.....	26
3.1. Design Space Formulation.....	26
3.1.1. Aerodynamic Performance	26
3.1.2. Drag Polar.....	28
3.2. Flight Envelope Formulation	29
3.3. Electric Motor Efficiency Map	31
3.4. Propeller Efficiency Map Formulation.....	34
3.5. Propeller Noise Map Modeling.....	37
3.6. Geographical Considerations for Noise Mitigation	39
3.6.1. Noise Directivity.....	40
3.6.2. Noise Distance and Azimuth Angle Computation	41
3.6.3. Noise Sensitivity Index	44
3.7. Flight Envelope Overlay	44
4. Analysis and Results.....	46
4.1. Design Space	46
4.2. Flight Envelope	50
4.3. The Electric Motor and Propeller	56
4.3.1. Electric Motor Efficiency.....	57
4.3.2. Propeller Efficiency.....	59

4.3.3.	Combined Electric Motor and Propeller Efficiency.....	62
4.3.4.	Propeller Noise Mapping	65
4.3.5.	Geographical Considerations for Propeller Noise Mitigation.....	69
4.4.	Flight Envelope Overlay	76
4.4.1.	Efficiency.....	77
4.4.2.	Noise	78
5.	Conclusion	80
5.1.	Significant Results.....	80
5.2.	Future Work.....	80
	REFERENCES	82

LIST OF TABLES

Table 2.1. Aerospace versus automotive design points	7
Table 2.2. Specific energy of different energy forms	14
Table 2.3. Specific energy of different energy forms with efficiency knockdown	14
Table 2.4. Gasoline engine and electric motor comparison.....	17
Table 2.5. Comparison of electric motors.....	18
Table 3.1. Hamilton Standard far-field propeller noise prediction inputs	39
Table 4.1. Design space variable definitions based on the Diamond HK-36	47
Table 4.2. Propeller and aircraft variable definitions for efficiency.....	60
Table 4.3. Propeller and aircraft variable definitions for noise	65
Table 4.4. Propeller and aircraft variable definitions for noise at a geographic location .	72
Table 4.5. Propeller and aircraft variable definitions for noise	74
Table 4.6. Diamond HK-36 noise and efficiency results.....	75

LIST OF FIGURES

Figure 2.1. NASA hybrid and electric road map	8
Figure 2.2. Top level of alternative propulsion classification tree	9
Figure 2.3. Serial hybrid system description	12
Figure 2.4. Volume and mass specific energy of different energy storage systems	15
Figure 2.5. Battery technology and expected development	16
Figure 2.6. Gasoline engine versus electric motor operation	19
Figure 2.7. Two kinds of fixed-pitch propellers versus a constant-speed propeller	21
Figure 2.8. Total system efficiency with typical component efficiencies	23
Figure 2.9. Turbofan engine with chevrons	25
Figure 3.1. YASA-750 motor and controller net efficiency	32
Figure 3.2. Maximum power and torque versus RPM	33
Figure 3.3. Noise at constant thrust	37
Figure 3.4. Noise at constant thrust based on blade pitch angle	38
Figure 3.5. Noise directivity	40
Figure 3.6. How the position of maximum noise can move at constant thrust	41
Figure 3.7. Representation of noise distance and azimuth	42
Figure 4.1. Diamond HK-36 100% hybrid design space	48
Figure 4.2. Diamond HK-36 90% hybrid design space	49
Figure 4.3. Diamond HK-36 100% to 90% hybrid comparison	50
Figure 4.4. Diamond HK-36 100% hybrid design space	51
Figure 4.5. Diamond HK-36 100% hybrid flight envelope	52
Figure 4.6. Diamond HK-36 100% and 90% hybrid flight envelope	53
Figure 4.7. Diamond HK-36 varying aerodynamic efficiency flight envelope	54
Figure 4.8. Diamond HK-36 varying battery specific energy flight envelope	55
Figure 4.9. Diamond HK-36 varying endurance flight envelope	56
Figure 4.10. Digitized YASA-750 efficiency map	57
Figure 4.11. YASA-750 efficiency map with operating limitations	58
Figure 4.12. Digitized propeller efficiency map	59
Figure 4.13. Propeller efficiency map	60
Figure 4.14. Propeller efficiency map with appropriate bounds	61
Figure 4.15. Electric motor and propeller efficiency overlay	62

Figure 4.16. Electric motor and propeller combined efficiency map	63
Figure 4.17. Combined efficiency with a constant thrust curve	64
Figure 4.18. Propeller noise map	66
Figure 4.19. Combined efficiency and propeller noise.....	67
Figure 4.20. Location of maximum efficiency and minimum noise at constant thrust	68
Figure 4.21. Map of the Daytona Beach, FL area.....	69
Figure 4.22. Noise sensitivity regions and applicable indices	70
Figure 4.23. Location of various NSIs at constant thrust	71
Figure 4.24. Geographical map of a Diamond HK-36 flyover	73
Figure 4.25. Efficiency and noise given aircraft and observer position	75
Figure 4.26. Diamond HK-36 100% hybrid flight envelope	76
Figure 4.27. Diamond HK-36 flight envelope maximum efficiency.....	78

SYMBOLS

\vec{A}	Vector pointing from the aircraft in the direction of its longitudinal axis
C_{D_0}	Base drag coefficient at $C_L = 0$
C_D	Drag coefficient
C_L	Lift coefficient
C_P	Coefficient of Power
C_Q	Coefficient of Torque
C_T	Coefficient of Thrust
D_p	Propeller diameter
L/D	Lift-to-drag ratio
\vec{O}	Vector pointing from the aircraft to an observer
P_{av}	Power available
P_{req}	Power required
W_E	Energy weight
W_{bat}	Battery weight
W_o	Aircraft gross weight
n_b	Number of blades per propeller
n_p	Number of propellers
A	Aspect ratio
D	Drag force
E	Endurance
H	Distance between two latitude and longitude pairs
J	Advance ratio
L	Lift force
P	Propeller power
Q	Propeller torque
R	Earth's radius
S	Wing area
T	Propeller thrust
V	Aircraft velocity
b	Wing span
d	Distance between an aircraft and an observer
dh	Distance between two altitudes
$dlat$	Distance between two latitudes
$dlon$	Distance between two longitudes
e	Oswald efficiency factor
h	Altitude
k	Induced drag correction factor
lat	Latitude
lon	Longitude
n	Revolutions per second
x	Percent hybrid

ϵ_{bat}	Battery specific energy
ϵ_{gas}	Gas specific energy
η_{bat}	Battery efficiency
η_{em}	Electric motor efficiency
η_{gen}	Generator efficiency
η_{gt}	Gas turbine efficiency
η_p	Propeller efficiency
β	Energy weight fraction
δ	Azimuth angle
θ	Pitch angle
λ	Central angle of the Earth
ρ	Air density
ϕ	Bank angle
ψ	Heading

ABBREVIATIONS

AC	Alternating current
ATAG	Air Transport Action Group
CAEP	Committee on Aviation Environmental Protection
DC	Direct current
EFRC	Eagle Flight Research Center
ERAU	Embry-Riddle Aeronautical University
FAA	Federal Aviation Administration
GA	General aviation
GAMA	General Aviation Manufacturers Association
GPS	Global Positioning System
ICAO	International Civil Aviation Organization
IMU	Inertial measurement unit
NASA	National Aeronautics and Space Administration
NED	North-East-Down
NSI	Noise sensitivity index
RPM	Revolutions per minute

ABSTRACT

Gartenberg, Lenny MSAE, Embry-Riddle Aeronautical University, May 2017. Battery Centric Serial Hybrid Aircraft Performance and Design Space.

The design space and flight envelope of a battery centric serial hybrid aircraft has been analytically derived. The formulation assumes cruising flight only and all energy available is used. The flight envelope can be generated for any conventional propeller driven serial hybrid aircraft. The advantageous combination of an electric motor and controllable-pitch electric propeller was also explored. The results are used to be able to control efficiency and noise at constant thrust and therefore constant airspeed. Manufacturer provided electric motor and propeller data is used for efficiency purposes. Since the electric motor is virtually silent compared to the propeller, published noise evaluation methods are used to estimate the noise footprint of the propeller.

Serial hybrid aircraft are appealing for their expansion of the flight envelope compared to fully electric aircraft and for their potential to operate where gasoline engines alone cannot. A serial hybrid configuration also allows for a controlled efficiency output and noise footprint to be able to either reduce emissions and cost or mitigate noise over noise sensitive areas. While a fully electric aircraft can achieve the efficiency and noise solutions, the serial hybrid solution offers considerably better range and endurance, making it viable for longer haul flights at higher airspeeds.

1. Introduction

1.1. Motivation

General aviation (GA) aircraft emissions and noise are a continuously growing problem around the world. The Federal Aviation Administration (FAA) predicts that GA operations (which currently account for 52% of operations in 2015) are going to increase an average of 0.3% per year in the United States. This increase in operations is predicted to have an increase in hours flown by 1.2% per year through 2036 (FAA, 2016). As the number of flight operations and flight times increase, so does the impact to the environment.

Aircraft efficiency plays a large role with respect to the environment. According to the General Aviation Manufacturers Association (GAMA), GA fuel consumption has increased nearly 25% from 2000 to 2013 and is predicted to increase another 70% through 2034 (GAMA, 2014). The increase of fuel consumption leads to an escalation in emissions. One way to mitigate this would be to continually improving the existing technology and engineering more fuel efficient airplanes. However, as the airplanes and their engines become more fuel efficient, there will also be more of them in the sky. For example, the Air Transport Action Group (ATAG) has a target of improving fleet fuel efficiency by 1.5% per annum between 2016 and 2020. (ATAG, 2016). While this is an attainable goal, the net emissions released into the atmosphere may not share the same benefit since the FAA predicts a 1.0% increase in fleet size per annum during the same time frame (FAA, 2016).

The cost of fuel plays into why efficiency matters as well. Over the last decade, fuel prices have had a great deal of volatility, driving the operating cost up and down with the

market. Highly efficient modern aircraft would not see as much of this burden as older, less efficient aircraft would. It is important to note that the efficiency range referred to is from 20% to 40% efficient. Regardless of the actual value, a significant amount of fuel, and therefore money, is wasted into another form of energy that does contribute to aircraft performance. A 1.5% increase in efficiency per year is an improvement, however, gas prices have the ability to escalate much faster, outweighing the cost benefit of a more efficient, modern airplane.

Aviation noise has historically been one of the most significant sources for community complaints around airports. The Committee on Aviation Environmental Protection (CAEP) found that a day-night average sound level of 75 dB is not only found to be an annoyance by 37% of the population, but it can also lead to other health issues such as sleep disturbance, hypertension, and mental health effects (CAEP, 2010). As a result, housing values can depreciate up to 10% in these residential areas as well as rental loss. Many airports around the United States have developed procedures for noise abatement. For example, Santa Monica Municipal Airport in California does not allow certain types of aircraft to operate at the airfield. As for the aircraft that can operate, repeat offenders of the noise limit are subject to fines or suspension from using the airport (Santa Monica Municipal Airport, 2016). Boca Raton Airport in Florida has voluntary noise restrictions and abatement procedures in place in an effort to mitigate aircraft noise as to not disturb the highly populated surrounding communities. These procedures include using specific headings and altitudes to avoid overflight of residential areas. The airport also has a night-time voluntary curfew to cease all aircraft operations at the airport (Boca Raton Airport, 2016). Pilots flying into or out of Boca Raton are requested to divert from their

flight plan to follow noise abatement procedures as well as restrict night and weekend flight operations.

The International Civil Aviation Organization (ICAO) assists on the development and standardization of low noise operational procedures that are safe and cost effective. The possibilities include preferential runways and routes as well as noise abatement procedures for takeoff and landing to minimize community noise. The physical layout of the airport and its surroundings dictate the appropriate measure that is to be used. In all cases, the procedure must give priority to safety considerations (ICAO, 2016).

Fully electric aircraft have become a central research point to try to solve aircraft efficiency and noise problems. Electric motors are a great candidate since they can exceed 95% efficiency, are essentially silent, readily available, and very cheap to obtain. Considering only the cost of energy and with respect to automobiles, the cost per unit of energy in the form of electricity is roughly half of that from its gasoline counterpart (U.S. Department of Energy, 2016). While the ratio is not directly applicable to aircraft, this trend can be approximated in that it will cost significantly less to operate an electric aircraft than a gasoline aircraft. The environmental toll is also significantly reduced since there are many alternative and clean ways to obtain electricity. These include, but are not limited to, hydroelectric, solar, and wind. The use of these renewable energy sources will help further cut emissions since the energy is extracted from nature instead of a combustion process.

Embry-Riddle Aeronautical University's (ERAU) Eagle Flight Research Center (EFRC) is at the forefront of electric aircraft technology by developing their own fully electric airplane converted from a Diamond HK-36 airframe dubbed the "e-Spirit of St. Louis". The EFRC is working with Powering Imagination and the National Park Service

to achieve this goal with the intention of obtaining the first FAA issued type certificate for an electric airplane. The airplane will be powered using off the shelf batteries as its only energy source. While the electric airplane will help solve the efficiency and noise dilemma of aircraft, the nature of the battery presents new problems: range and airspeed. The best batteries commercially available to date contain only a fraction of the specific energy of gasoline, imposing these limitations. The most viable way to overcome these limitations is to use a hybrid electric aircraft that is part gasoline, part battery. This opens the door to a wide variety of design solutions for larger aircraft.

In conjunction with fully electric research, the EFRC is also leading a Hybrid Electric Research Consortium, whose membership includes Airbus, General Electric Aviation, Argonne National Lab, Hartzell Propeller, Pratt and Whitney Canada, Rolls-Royce Liberty, and Textron Aviation. The consortium is investigating a hybrid electric aircraft solution that can carry nine (9) passengers and is propeller powered to replace existing gasoline turboprop aircraft.

1.2. Problem Statement

The development of hybrid aircraft is gaining substantial interest in the aviation industry. Hybrid aircraft have the potential to be more efficient and quieter than their gas piston or turbine engine counterpart. This thesis emphasizes the exploration of battery centric serial hybrid propeller powered aircraft. The design space and flight envelope of this type of aircraft needs to be defined based on top level aircraft parameters as well as hybridization. Efficiency and noise for an electric motor and controllable-pitch propeller are also evaluated since they offer a new combination of components that generate thrust.

1.3. Objectives

1.3.1. General Objective

The primary objective of this work is to develop a serial hybrid aircraft design space and flight envelope with emphasis on efficiency and noise. The design space and flight envelope are analytically derived and have closed-form solutions for given aircraft parameters. The analysis, however, assumes the aircraft is propeller driven for thrust. It is also desired to be able to mathematically compute the net efficiency and noise at a given operating point within the flight envelope for a more detailed analysis and optimization.

1.3.2. Specific Objectives

Quantify the impact of aerodynamic improvements.

Modern aerodynamics have ample opportunity for improvement. Motor gliders take advantage of improved aerodynamics, but are light weight and typically carry a pilot and passenger. Improving the aerodynamics of a larger turboprop aircraft can considerably improve performance. While this is independent from the concept of a serial hybrid aircraft, the developed methods are used to be able to quantify the impact of improving aerodynamics.

Quantify the impact of battery specific energy improvements.

Battery technology changes and its specific energy improves marginally every year. Despite this improvement, fuel comprises a significantly higher specific energy. As a result, batteries limit the flight envelope which can be observed in present day fully electric aircraft. Most of these aircraft can only fly at low speeds and for short periods of time. It

is therefore required to demonstrate the impact of battery specific energy and how it can vastly improve the flight envelope.

Identification of the advantageous combination of an electric motor and controllable-pitch propeller.

Electric motors are typically designed for ground applications, but offer significant advantages in an aircraft operation. While aircraft gasoline engines have a defined torque versus RPM curve, electric motors allow for its operation to be off of this curve and can produce the same power output and many torque and RPM combinations. The controllable-pitch propeller compliments the electric motor well since it is not tied to a specific torque and RPM combination. The identification and use of torque, RPM, and propeller pitch is a necessity for hybrid aircraft.

Optimize efficiency and/or noise at a given altitude and airspeed.

The operating torque versus RPM constraint is relaxed for electric motors and can be varied to produce the same power or thrust output with the combination of an electric motor and controllable-pitch propeller. Electric motors have wide operating regions of very high efficiency. Controllable-pitch propellers have a narrow high efficiency range where some flight conditions will produce higher propeller efficiency than others. Propeller noise is a function of power, airspeed, and altitude, while the electric motor is virtually silent in comparison. It is desired to combine the electric motor and propeller to be able to optimize both for a given altitude and airspeed taking propeller noise output into consideration.

2. Literature Review

2.1. Alternative Propulsion

Modern aircraft research is looking into alternative fuels or battery power as their means of alternative propulsion. While this is currently implemented in the automotive industry, the aerospace industry requires a different design space. In aircraft design, it may be desirable to minimize cost, volume, and weight. However, unlike the automotive industry, weight has a real physical limitation in the design of an airplane and becomes one of the top priority considerations. Cost is also a factor in aircraft design, however, when a GA aircraft can exceed \$1,000,000 in purchase price, an extra few thousand dollars is less than 1% additional cost and ultimately will not impact aircraft sales. Modern airplanes also contain a noteworthy amount of unused volume that can hold less dense fuels or batteries.

Table 2.1. Aerospace versus automotive design points

Industry	Cost	Weight	Volume
Automotive	Critical	Low	High
Aerospace	Low	Critical	Low

Alternative propulsion research is underway in both federal agencies and private industry. The National Aeronautics and Space Administration (NASA) is leading a United States effort to produce viable electric and hybrid electric aircraft technology.

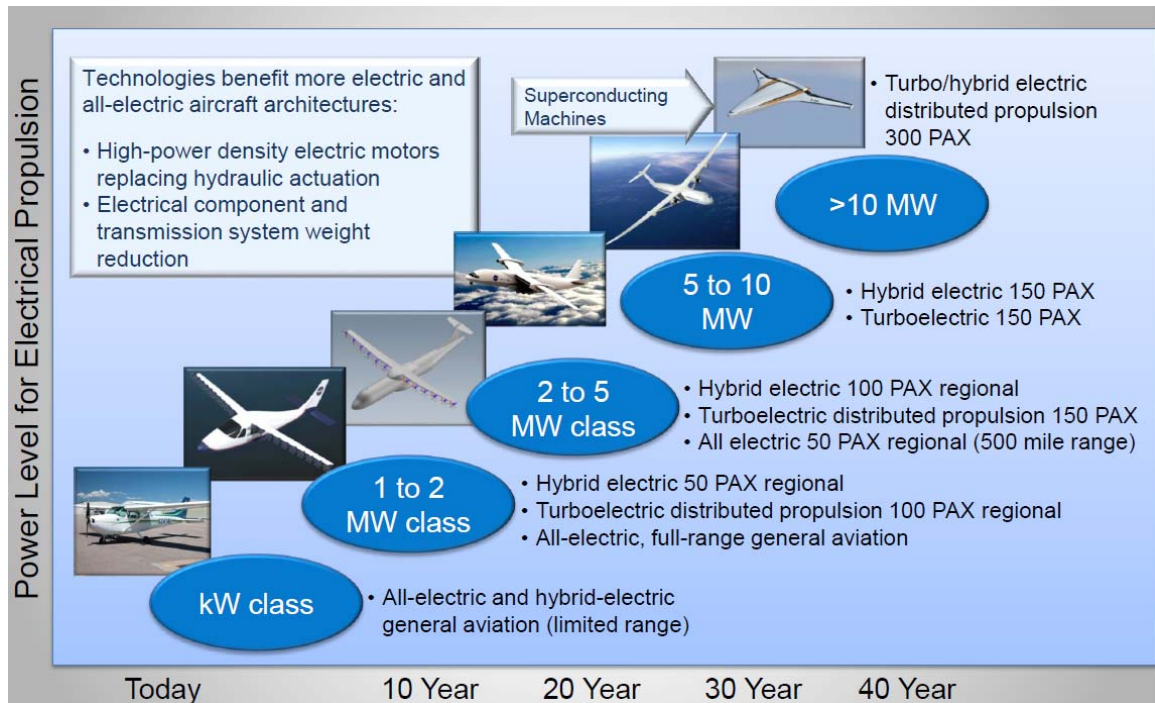


Figure 2.1. NASA hybrid and electric road map (Clarke, 2015)

NASA's Neil A. Armstrong Flight Research Center is leading this effort, starting in the kilowatt (kW) class of aircraft with the X-57 Maxwell (formerly known as SCEPTOR). The goals of this program are to reduce total operating cost by 30%, produce zero in-flight carbon emissions, reduce community noise by 15 dB, and create a certification basis for distributed electric propulsion (Clarke, 2016). The X-57 is a stepping stone towards the future of alternative propulsion with the ultimate goal of scaling the technology to commercial size airliners.

Alternative propulsion is a broad term for the technology. This expression is merely a high level description of new areas of research. A classification tree can be used to visualize the different types of alternative propulsion systems as shown in Figure 2.2. Alternative propulsion for this discussion is broken down into three (3) types per Figure 2.2: combustion, hybrid electric, and fully electric.

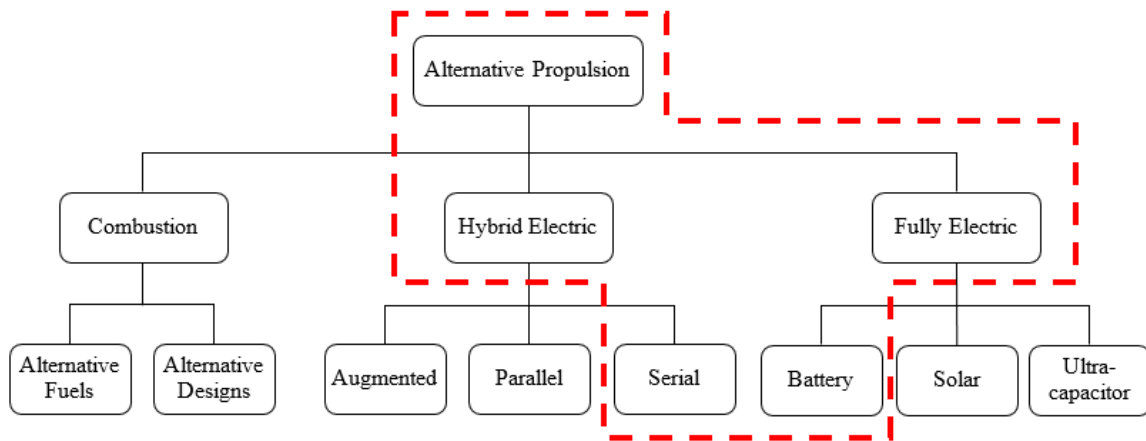


Figure 2.2. Top level of alternative propulsion classification tree (Marwa, 2016)

While all branches of the classification tree can help reduce emissions, noise, direct operating costs, or a combination of them, some branches are better suited to deal with certain operations than others. All of these branches will be briefly discussed, but the emphasis for this thesis is outlined by the red dashed box.

A combustive form of alternative propulsion is the simplest way to reduce emissions. This comes through either alternative fuels or designs. Both industry and academia are well-versed with the type of modifications and redesigns necessary to reduce fuel burn and therefore emissions and cost. However, this branch does not present a solution to the noise problem.

Fully electric propulsion has the capability to reduce emissions, noise, and direct operating costs. Electricity is a renewable form of energy which can be obtained and stored in a variety of ways, making it the most efficient form of alternative propulsion in Figure 2.2. The shortfall of fully electric propulsion is that it is currently only capable of operating at low airspeed. If the aircraft also does not have solar panels or any other means of

generating electricity, range is also severely limited. With respect to aircraft, slow speed and short range typically do not fall under a desired mission.

Hybrid electric propulsion is capable of not only the reduction of emissions, noise and direct operating costs, but it also have the potential to fly faster and over longer distances. Hybrid electric can be further broken down into parallel and serial hybrid. For discussion purposes, it is assumed that hybrid electric propulsion consists of a gasoline engine component and an electric motor component.

A parallel hybrid configuration is characterized by a gasoline engine and an electric motor that are capable of generating shaft horsepower physically connected by a gearbox, torque converter, or clutch assembly. Parallel hybrid is generally better for direct operating costs with a hub-to-hub type of mission. This means that a parallel hybrid aircraft is a better selection for a long distance flight that operates at higher altitudes similar to present day airline operations.

A serial hybrid configuration is one in which there is a single path towards producing thrust. Serial hybrid is the ideal candidate for door-to-door missions since they are a better choice for noise. A door-to-door mission is defined as an aircraft operation that flies locally for everyday life such as a commute to and from work. These operations will naturally fly lower which makes noise consideration a critical design component for this type of aircraft.

While all types of alternative propulsion have their respective set of advantages and disadvantages, this work will only focus on research towards a serial hybrid solution. Recall the red dashed box in Figure 2.2. The serial hybrid and battery powered fully electric branches are both included since a serial hybrid aircraft can operate like a fully electric

aircraft when the gasoline engine component is not in use.

2.2. Serial Hybrid

A serial hybrid propulsion system is one that has only a single path towards producing thrust for the aircraft. These systems are typically classified by a conventional engine attached to a generator, which is connected to battery capacitance that then feeds to an electric motor to power the propeller. A gearbox may also be used to control the relationship between the motor RPM and the propeller RPM.

The serial hybrid configuration can be operated in three different ways. The first way is to use only the battery energy to power the electric motor and propeller. During this operation, the system is essentially an electric aircraft and is highly efficient, produces no carbon emissions, and is quiet. This requires the batteries to be charged on the ground prior to the flight by plugging the aircraft into a power socket. However, batteries have a limited capacity which reduces its range and endurance. The second mode of operation is to use a gas turbine to produce electricity through a generator and feed this directly into the electric motor. At this point, inefficiencies begin to stack so there will be a reduced benefit, but range and endurance are significantly extended due to the specific energy of gas. The third method of operation is to use the serial hybrid in an air charging configuration. This mode of operation uses a portion of the gas turbine power to charge the batteries while the other portion feeds to the electric motor to sustain thrust. This process greatly stacks inefficiencies since all systems are operating simultaneously and additional power is required from the gas turbine to charge the batteries. Once the batteries are charged to a defined threshold, the gas turbine could theoretically power back and the airplane can resume flight under fully electric operation. All three modes of operation are illustrated in

detail in Figure 2.3.

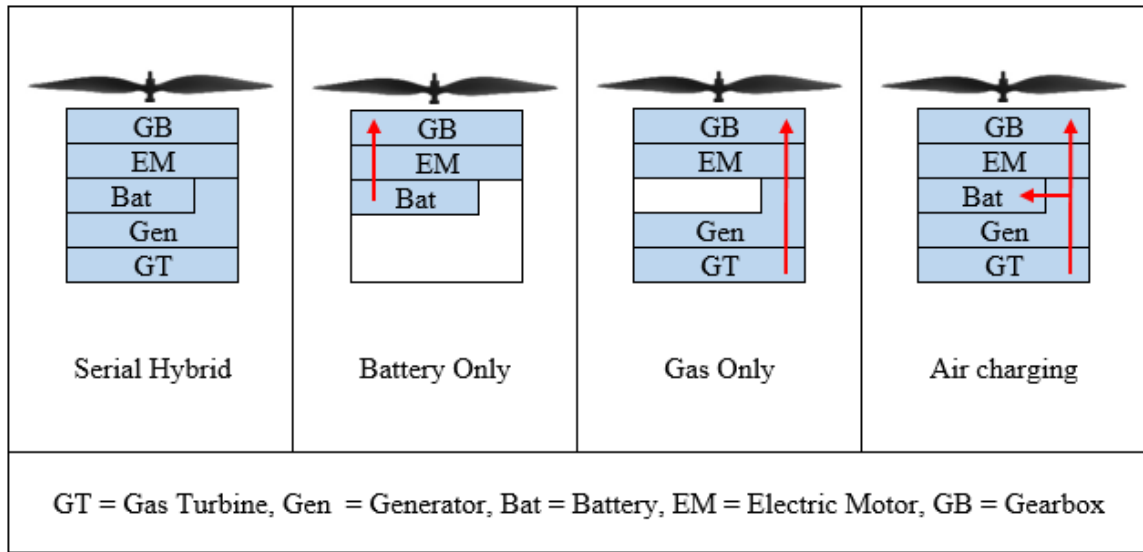


Figure 2.3. Serial hybrid system description (Marwa, 2016)

Several attempts have been made to estimate the range of a serial hybrid electric aircraft. Equation (2.1) (Marwa, 2016) will be used as the reference equation for future derivations. A key component of this equation is how the specific energies of gas and batteries are blended together and can break down into the Breguet range equation.

$$R = \frac{\eta_p L}{g D} \left[\eta_{em} \eta_{bat} \epsilon_{bat} x \beta + \eta_{gt} \eta_{gen} \eta_{em} \epsilon_{gas} \ln \left(\frac{1}{1 - (1 - x) \beta} \right) \right] \quad (2.1)$$

This equation requires the definition of the percent hybrid parameter (x) and the energy weight fraction (β). An airplane drawing energy from gas alone is considered 0% hybrid ($x = 0$) while an airplane that is fully electric is considered 100% hybrid ($x = 1$). The percent hybrid parameter is therefore a value between zero (0) and one (1) which defines how much of the energy weight fraction is batteries and how much is gas. The energy weight fraction is analogous to the typical gasoline aircraft fuel weight fraction in that it

defines what percentage of the weight of the airplane is used for energy storage. This value also falls between zero (0) and one (1). It is important to note that Equation (2.1) breaks down to the standard Breguet range equation most commonly found in literature using either 0% hybrid for a gas airplane or 100% hybrid for an electric airplane. The other terms of this equation are the various component efficiencies, battery and gas specific energies, and the lift-to-drag ratio.

2.3. Batteries

There are two types of batteries available on the market today, primary and secondary batteries. The primary battery is not rechargeable and limited to a one time use. The secondary battery is rechargeable and can be cycled multiple times. The foregoing serial hybrid electric aircraft design will only consider the secondary battery type.

Batteries can come in various shapes along with different chemistries. While different batteries offer different advantages, when considering a hybrid aircraft, it is desired to be able to have the most available energy with the least amount of weight (maximize specific energy). This narrows the choice down to an 18650 lithium ion cylindrical cell. The name 18650 represents the size of the battery, meaning an 18 mm diameter and a 65 mm height. These cells typically weigh around 50 grams making them very light. While the weight is relatively low, batteries are not capable of holding large amounts of energy. It is important to be able to compare the specific energy of the battery to that of gas.

Table 2.2. Specific energy of different energy forms

Energy Source	Specific Energy (hp-hr/lbf)	Comparison to 100LL
Avgas (100LL)	7.43	-
Jet A	7.27	97.8%
Sanyo 18650GA	0.16	2.2%

Referring to Table 2.2, it is apparent that the battery severely lacks in specific energy. Nonetheless, there is one other consideration before jumping to a conclusion about the usefulness of a battery when compared with gas. An efficiency knockdown can be applied to each of the energy sources as a representation of how efficient each source's energy conversion process is. This knockdown value reduces the energy source's effective specific energy and allows for a direct comparison of which source has the highest specific energy.

Table 2.3. Specific energy of different energy forms with efficiency knockdown

Energy Source	Knockdown	Specific Energy (hp-hr/lbf)	Comparison to 100LL
Avgas (100LL)	35%	2.60	-
Jet A	35%	2.54	97.8%
Sanyo 18650GA	92%	0.15	5.7%

Table 2.3 portrays that when considering the inefficiencies, the energy storage per unit weight of gas is still roughly seventeen (17) times better than that of batteries. This creates a significant issue when using this type of energy in aircraft since the airplane must weigh more to hold the same amount of energy. Hybrid electric aircraft help mitigate this issue since there will still be some gas available. While the efficiency is improved and noise is reduced, they do so at the expense of range and endurance.

A driving factor in the push for using battery technology is that batteries are projected to get better each year whereas gas does not. These improvements include

reducing the cost per cell, increasing the energy in each cell, reducing volume, and improving safety. While safety and cost are both significant issues for aircraft, only the energy and volume are considered here for further analysis.

Figure 2.4 clearly shows that while ethanol, methanol, and kerosene (gasolines) are currently more advantageous to use in terms energy per unit weight and volume, they are fixed at their respective points. Even though lithium hydroxide (LiOH) batteries are not the same as the lithium ion cells previously mentioned, they follow the same trend in that their specific energy can improve over time. Some battery chemistries may evolve faster than others, however, there is also the possibility that a given chemistry will not be better than another chemistry.

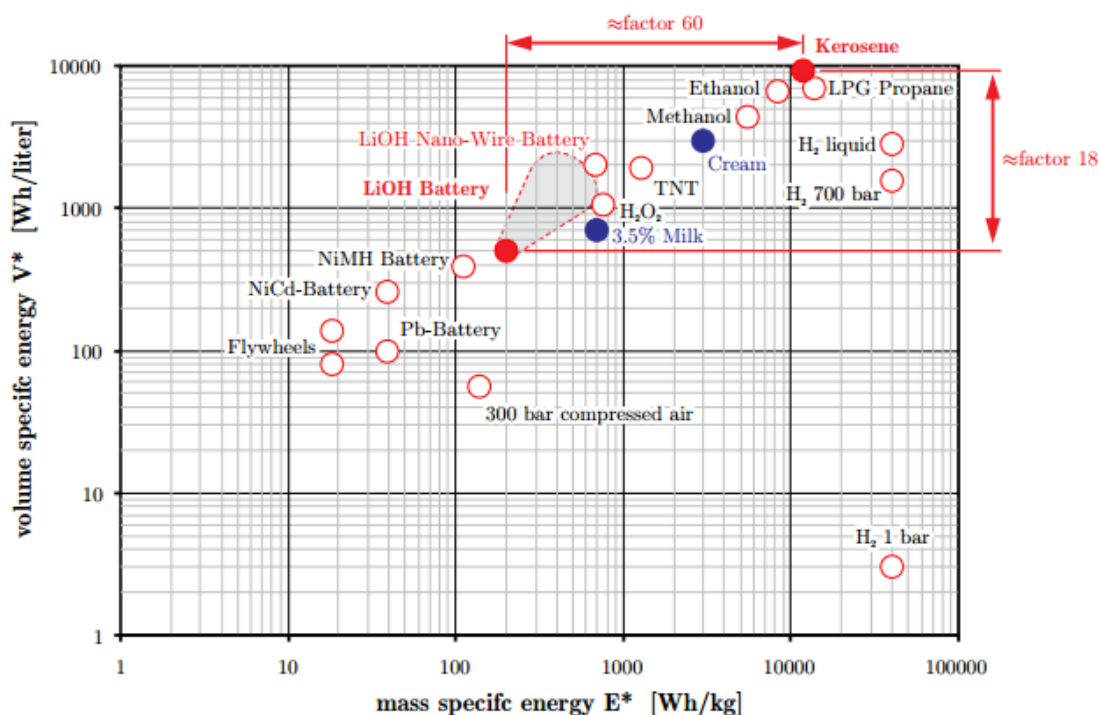


Figure 2.4. Volume and mass specific energy of different energy storage systems (Hepperle, 2012)

Even though battery specific energy is improving, it may not necessarily ever reach the specific energy of gas. As a comparison, gas would be roughly equivalent to the end of Figure 2.5 at 4000 Wh/kg after an efficiency knockdown. Batteries may be several decades away from being able to compete with gas in terms of specific energy, however, they are a good, variable, source of energy to utilize in a hybrid electric airplane as a means of upgrading the airplane as battery technology improves.

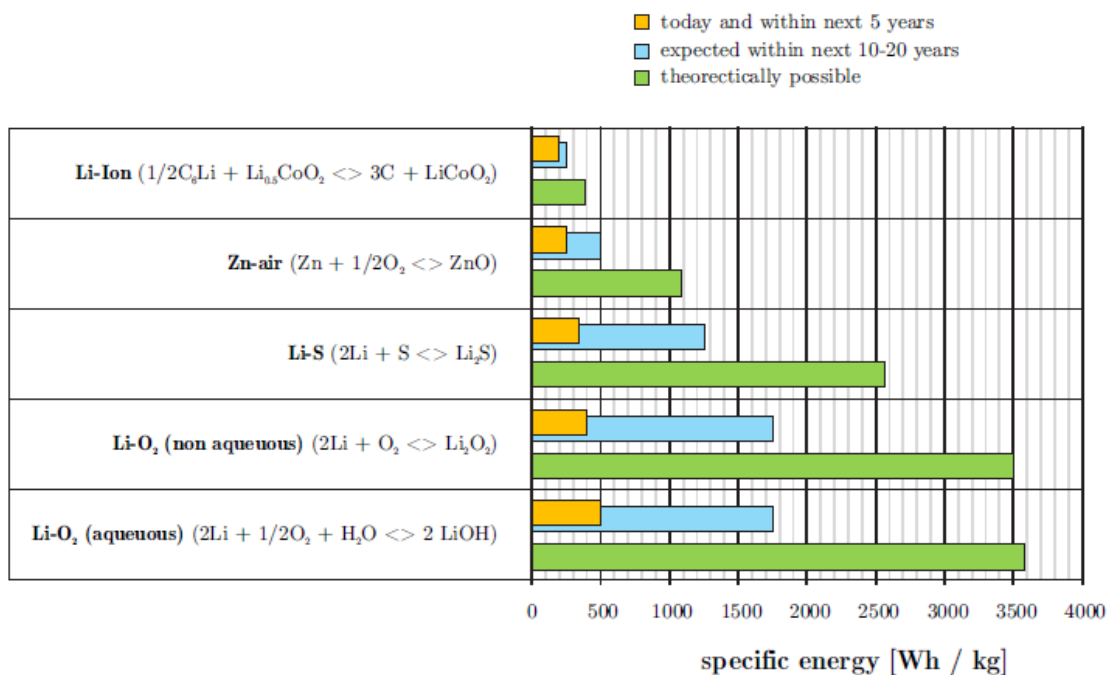


Figure 2.5. Battery technology and expected development (Hepperle, 2012)

2.4. Electric Motors

Electric propulsion in aviation historically has a very slow growth rate due to several factors: FAA regulations, battery technology, and slow change within the industry. Currently, all electric propulsion makes use of electric motors. While the regulations are strict and a significant amount of time and money is required to advance electric propulsion

commercially, electric motors offer many benefits that gasoline engines are unable to compete with. There are already several electric motors in the automotive industry that can be applied to aircraft. They are relatively light, very efficient, compact, and stackable in series for increased horsepower. Many of these motors operate at a torque and RPM range that is comparable to that of classical aircraft engines for direct propeller use.

Table 2.4. Gasoline engine and electric motor comparison

Parameter	Gasoline Engine/Turbine	Electric Motor
Complexity	High	Low
Weight	High	Low
Efficiency	Low	High
Cost	High	Low
Maintenance	High	Low
Environmental Impacts	High	Low
Specific Power	Medium	High
Power Output	High	Low

Table 2.4 clearly shows that modern electric motors are better than their gasoline counterparts in a variety of ways with the exception of net power output. However, as technology improves, there is plenty of potential for electric motors to meet if not exceed the power output of gasoline engines.

There are many subcategories of electric motors that are application dependent. At the highest level, it is important to be able to compare an alternating current (AC) motor with a direct current (DC) motor. Within an AC motor, there also lies the options for single-phase and multi-phase current. Both AC and DC motors can be brushed or brushless. The following comparison assumes that the motor is to be used in an aircraft and has batteries as its power source.

Table 2.5. Comparison of electric motors (Costello, 2011) (Fehrenbacher, 2011)

Motor	Pros	Cons
AC Single-Phase	<ul style="list-style-type: none"> • Good for low power settings • Easier to maintain than multi-phase 	<ul style="list-style-type: none"> • Requires inverter • Less efficient than multi-phase • Discontinuous input power
AC Multi-Phase	<ul style="list-style-type: none"> • Good for high power settings • More efficient than single-phase 	<ul style="list-style-type: none"> • Requires inverter • More expensive than single-phase
DC	<ul style="list-style-type: none"> • Easy to control • Less rotor heat • No inverter losses 	<ul style="list-style-type: none"> • More expensive than AC
Brushed	<ul style="list-style-type: none"> • Cheaper and easier to manufacture than brushless • Simplicity of control • Simplicity of maintenance 	<ul style="list-style-type: none"> • Brushes can wear down and break • Continuous maintenance • Speed/torque less optimized • Poor heat dissipation
Brushless	<ul style="list-style-type: none"> • Low maintenance • High efficiency • High speed range • More controllable speed/torque settings 	<ul style="list-style-type: none"> • Costs more than brushed • Requires more complex speed control • Requires rotor position sensor or position synthesis

A gasoline engine operates on a fixed torque versus RPM curve while any electric motor with an appropriate controller can vary torque and RPM independently. Therefore, a gasoline engine has a single operating point for a required power output while an electric motor can have many torque and RPM combinations as shown in Figure 2.6.

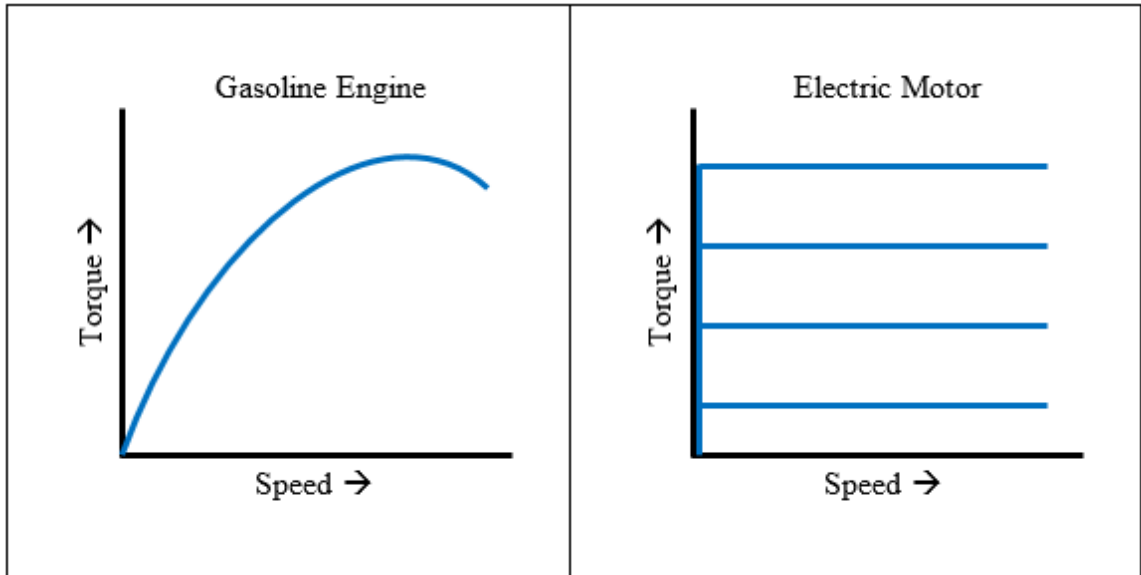


Figure 2.6. Gasoline engine versus electric motor operation

The electric motor benefit will come into play significantly when a controllable-pitch propeller is attached.

The EFRC is currently using a YASA-750 motor for their electric HK-36. The YASA-750 is a 3-phase, permanent magnet synchronous brushless motor that is optimized to operate on both 400 volt and 800 volt systems. All motors of this type require an inverter or motor controller to take the battery current and convert it into usable 3-phase AC form. The motor controller not only provides power to the motor, it also monitors the states of the electric motor and determines the proper phase switching sequence. Additionally, it may provide information to the operator in terms of torque, RPM, temperature, voltage, and current.

2.5. Propeller Theory

Aircraft propellers are used to generate a thrust force through lifting surfaces known as propeller blades. Propellers can be driven by piston engines, gas turbine (turboprop) engines, or electric motors and can operate as fixed-pitch, ground-adjustable, two-position, controllable-pitch, constant-speed, feathering, and/or reversing (Gudmundsson, 2014). While it is important to note that propellers can be operated in a variety of ways, only the cases of fixed-pitch and controllable-pitch propellers will be discussed in detail.

A fixed-pitch propeller is one in which the blade pitch angle is permanently fixed. This means that while the propeller is very simple and inexpensive, the best efficiency is only achieved at one airspeed. This is not a very practical solution as a typical mission profile requires various airspeeds. Therefore, the propeller can be designed for a typical cruising airspeed but will perform poorly during takeoff, climb, and descent. The solution to this single airspeed peak efficiency issue is to use a controllable-pitch or constant-speed propeller. These two terms are analogous to one another since either mode of operation can be used to achieve the same operating conditions and efficiency. The controllable-pitch propeller allows a pilot to change the propeller blade angle and RPM in order to maximize efficiency at a variety of airspeeds. Figure 2.7 clearly demonstrates how advantageous from an efficiency standpoint a constant-speed (controllable-pitch) propeller is. Regardless of the flight segment, propeller efficiency can be maximized to reduce the use of energy.

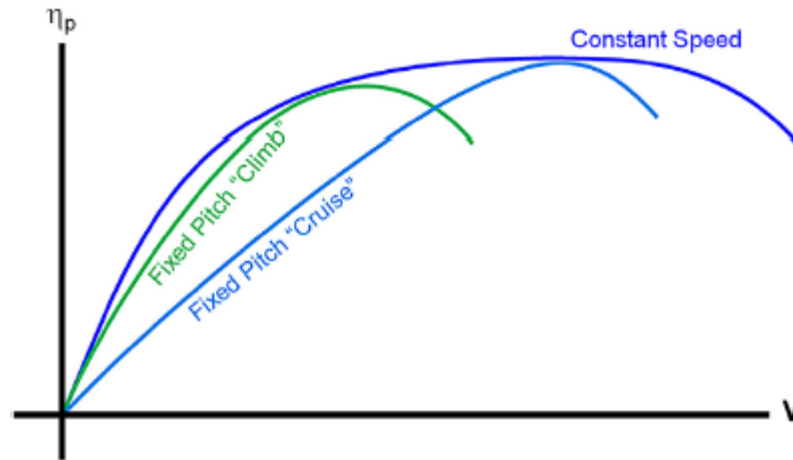


Figure 2.7. Two kinds of fixed-pitch propellers versus a constant-speed propeller (Gudmundsson, 2014)

Propeller power, thrust, torque, and efficiency are all related through a set of nondimensionalized equations.

Advance Ratio:

$$J = \frac{V}{nD_p} \quad (2.2)$$

Coefficient of Power:

$$C_P = \frac{P}{\rho n^3 D_p^5} \quad (2.3)$$

Coefficient of Torque:

$$C_Q = \frac{Q}{\rho n^2 D_p^5} \quad (2.4)$$

Coefficient of Thrust:

$$C_T = \frac{T}{\rho n^2 D_p^4} \quad (2.5)$$

Propeller efficiency:

$$\eta_p = J \frac{C_T}{C_P} = J \frac{C_T}{C_Q} \frac{1}{2\pi} = \frac{TV}{P} \quad (2.6)$$

Propeller performance can be computed in a variety of ways, most notably through either momentum theory or blade element theory. Some manufacturers provide the propeller efficiency data in a table or mapped format in terms of advance ratio and power coefficient (Gudmundsson, 2014). This allows the efficiency to be read directly using linear interpolation as necessary.

Serial hybrid aircraft can make great use of controllable-pitch propellers due to the nature of electric motors previously discussed. Current propellers are designed for traditional gasoline engines that have a fixed torque versus RPM curve, limiting the entire system to a single fixed curve. Variable torque versus RPM curves provided through an electric motor allow for interesting changes in propeller design. For example, an aircraft can make the same thrust at multiple RPMs by using the controllable-pitch propeller and electric motor combination. This combination has effects on propeller efficiency and noise that are only beginning to be explored.

2.6. Aircraft Efficiency

Aircraft efficiency has improved over 80% since the 1960s while engine fuel consumption has decreased nearly 50%. Even though these are staggering improvements, there is still considerably more room for improvement. These improvements come from the subtle differences in aircraft technology that a casual observer may not see. These include, but are not limited to, drag reduction, winglets, systems, composites, paint, and

engine design (ATAG, 2010). Hybrid and electric aircraft encompass a substantial efficiency boost without taking these technologies into account.

Based on Figure 2.8, fully electric airplanes are about twice as efficient as their gas counterpart in terms of energy conversion from its energy source to the aircraft's propeller. Note that Figure 2.8 assumes comparative efficiency values. Hybrid electric airplanes will contain both a kerosene and battery efficiency chain, so it is still ideal to be able to minimize weight and reduce fuel burn using other methods.

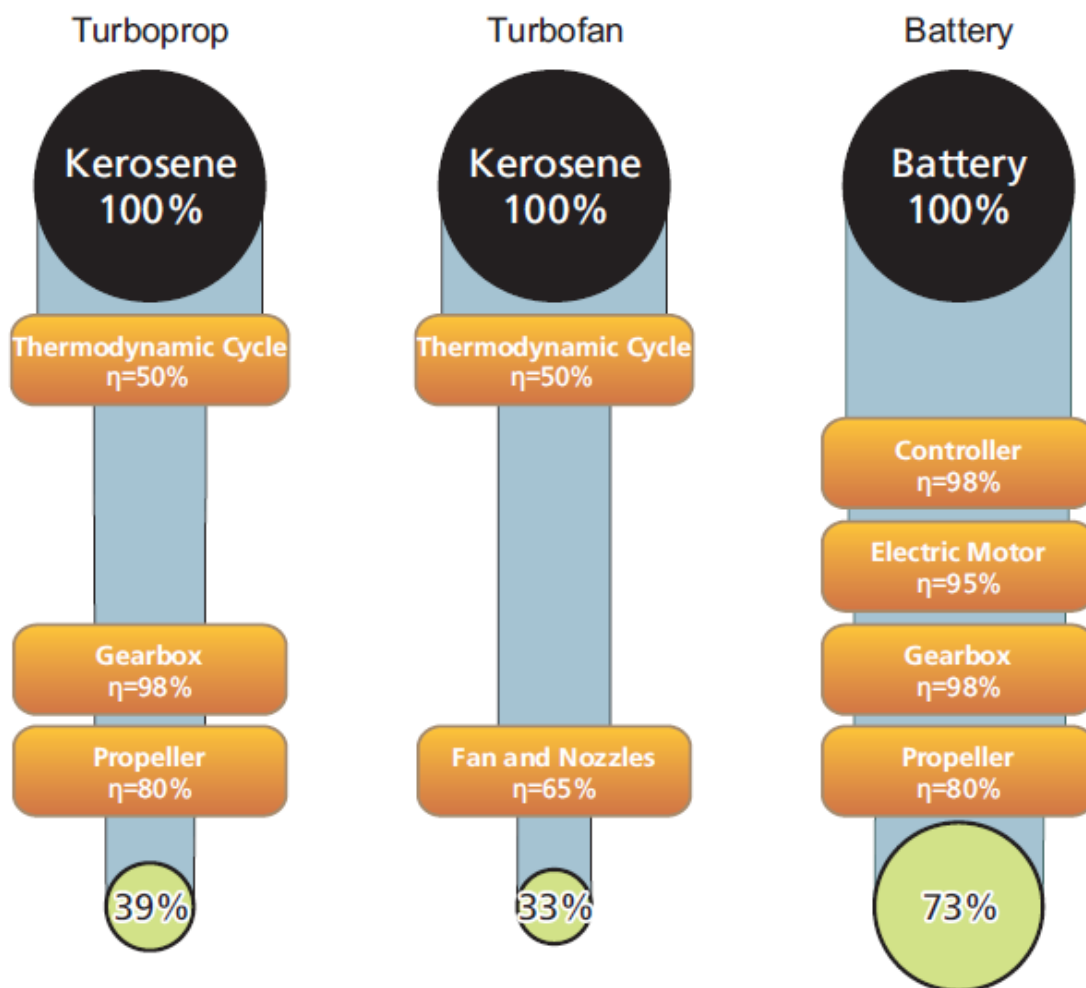


Figure 2.8. Total system efficiency with typical component efficiencies (Hepperle, 2012)

ATAG has provided some insight into how much fuel can be saved by employing various methods. Winglets alone have proven to reduce fuel consumption up to 5% without any major increase in wingspan. Reducing the weight of an aircraft equates to reducing the fuel used since less power is required. Modern aircraft are transitioning towards composites instead of traditional aluminum alloys. Carbon composites provide a much better strength-to-weight ratio than metals, sometimes as much as 20%. Even aircraft paint has its place in reducing weight. ATAG estimates that new paints will be available soon that weigh between 10% and 20% less than current paints (ATAG, 2010). All of these concepts can be applied to hybrid aircraft as well to help boost their efficiency further. However, none of these methods use the fact that there is an entirely new type of propulsion system on the airplane, that being electrical propulsion.

2.7. Aircraft Noise

Aircraft noise has become an ever increasing issue as air traffic continues to grow. Many locations around the United States practice noise abatement procedures near large communities and over national parks. These procedures do not necessarily solve the problem as the aircraft is still noisy but only restricts where the noise can exist on the ground.

Aircraft noise comes from four primary sources: aerodynamics, engines, propellers, and other systems. Hybrid electric aircraft will most likely be unable to solve aerodynamic noise or system noise such as landing gear or flap retraction. The main benefit will be achieved by reducing engine and propeller noise. Turbofan engines currently use chevrons on their trailing edge to help mitigate jet noise as shown in Figure 2.9.



Figure 2.9. Turbofan engine with chevrons

Aircraft that use these engines typically fly at high altitudes and land at large commercial airports where noise is expected. Simple solutions for propeller driven aircraft include using more propellers or blades to be able to reduce the blade diameter and consequently reducing the propeller tip speed which reduces noise. However, small GA aircraft still use full power for takeoff which maximizes engine and propeller RPM. Electric motor usage reduces the engine noise to virtually zero so most of the noise is generated by the propeller.

Hamilton Standard has developed an empirical method to predict far-field propeller noise based on available propeller test data in 1971 for preliminary design studies. This method uses nothing more than basic propeller geometry, aircraft states, atmospheric conditions, number of propellers, and number of propeller blades. An estimated perceived noise level is computed based on a series of partial levels and correction factors as well the distance and angle from the propeller's rotational axis (SAE, 1977).

3. Methodology

3.1. Design Space Formulation

3.1.1. Aerodynamic Performance

It is desirable to formulate a relationship between the lift-to-drag ratio, endurance, cruise speed, specific energy of batteries, specific energy of gas, energy weight fraction, and percent hybrid. For simplicity, it will be easier to begin assuming a fully electric aircraft and thereby removing any gas and percent hybrid terms that would be required otherwise. Recall the power required for a given propeller driven aircraft creating drag:

$$P_{req} = \frac{DV}{\eta_p} \quad (3.1)$$

Assuming weight and lift are equal for level flight:

$$W_o = L \quad (3.2)$$

For which Equation (3.1) can be rewritten in a more convenient form:

$$P_{req} = \frac{1}{\eta_p} V \left(\frac{L}{D} \right)^{-1} W_o \quad (3.3)$$

This is a statement of the power required of an aircraft with a given aerodynamic efficiency. Now, the power available for a battery powered electric propulsion system needs to be defined. In this case, power is a function of the specific energy of the battery (ϵ_{bat}), time (E), total weight of the batteries (W_{bat}), electric motor efficiency (η_{em}), and battery efficiency (η_{bat}):

$$P_{av} = \frac{\epsilon_{bat}}{E} W_{bat} \eta_{em} \eta_{bat} \quad (3.4)$$

Rewriting Equation (3.4) in terms of battery weight fraction (W_{bat}/W_o):

$$P_{av} = \eta_{em}\eta_{bat} \frac{\epsilon_{bat}}{E} \frac{W_{bat}}{W_o} W_o \quad (3.5)$$

And equating the power required from aerodynamics, Equation (3.3), to the power available from the electric propulsion system, Equation (3.5), for steady, level flight yields:

$$\frac{1}{\eta_p} V \left(\frac{L}{D}\right)^{-1} W_o = \eta_{em}\eta_{bat} \frac{\epsilon_{bat}}{E} \frac{W_{bat}}{W_o} W_o \quad (3.6)$$

Solving Equation (3.6) for L/D whereby eliminating gross weight produces:

$$\frac{L}{D} = \frac{VE}{\eta_p\eta_{em}\eta_{bat}} \frac{1}{\epsilon_{bat} \frac{W_{bat}}{W_o}} \quad (3.7)$$

For a given propeller and electric motor efficiency, battery weight fraction, and endurance, Equation (3.7) relates the required aerodynamic efficiency of the aircraft to the velocity. Therefore, a base is now provided to the aerodynamic performance required from an aircraft for a given battery specific energy.

Equation (3.7) currently assumes a fully electric aircraft under battery power, however, the goal is to be able to define this for a serial hybrid. To accomplish this, Equation (2.1) will be used to start the process and is repeated here for convenience:

$$R = \frac{\eta_p}{g} \frac{L}{D} \left[\eta_{em}\eta_{bat}\epsilon_{bat}x\beta + \eta_{gt}\eta_{gen}\eta_{em}\epsilon_{gas} \ln \left(\frac{1}{1 - (1-x)\beta} \right) \right] \quad (3.8)$$

Using the simple definition that range is the product of endurance and velocity, electric motor efficiency can be factored out of the equation resulting in an isolated L/D in terms of percent hybrid (x) and energy weight fraction (β):

$$\frac{L}{D} = \frac{VE}{\eta_p \eta_{em} \eta_{bat} \epsilon_{bat} x \beta + \eta_{gt} \eta_{gen} \epsilon_{gas} \ln \left(\frac{1}{1 - (1-x)\beta} \right)} \quad (3.9)$$

As it can be seen, Equations (3.7) and (3.9) are very similar to one another with the exception of the weight fraction and specific energy component. To prove that the equations are in fact identical, let the percent hybrid be equal to one (1) for a fully electric aircraft. Since the energy is now only from batteries, the energy weight fraction is the same as the battery weight fraction. Equation (3.9) becomes:

$$\frac{L}{D} = \frac{VE}{\eta_p \eta_{em} \eta_{bat} \epsilon_{bat} \frac{W_{bat}}{W_o} + \eta_{gt} \eta_{gen} \epsilon_{gas} \ln(1)} \quad (3.10)$$

The gas term drops out producing the final result identical to Equation (3.7):

$$\frac{L}{D} = \frac{VE}{\eta_p \eta_{em} \eta_{bat} \epsilon_{bat} \frac{W_{bat}}{W_o}} \quad (3.11)$$

By extension of the derivation, Equation (3.9) can be used to describe the aerodynamic performance required for a serial hybrid aircraft since it has a blended specific energy and energy weight fraction term for both gas and batteries compared to that of only batteries.

3.1.2. Drag Polar

The maximum aerodynamic performance is limited by its drag polar. A parabolic drag polar will be assumed:

$$C_D = C_{D_o} + kC_L^2 \quad (3.12)$$

Where:

$$k = \frac{1}{\pi e A} \quad (3.13)$$

The goal is to write the drag polar in terms of L/D . To start, take the reciprocal of the drag polar and multiply both sides by the lift coefficient:

$$\frac{C_L}{C_D} = \frac{C_L}{C_{D_o} + k C_L^2} \quad (3.14)$$

Dimensionalizing Equation (3.14) and applying Equations (3.2) and (3.13) yields:

$$\frac{L}{D} = \frac{\frac{W_o}{\frac{1}{2} \rho V^2 S}}{C_{D_o} + \frac{1}{\pi e A} \left(\frac{W_o}{\frac{1}{2} \rho V^2 S} \right)^2} \quad (3.15)$$

Substitute in the aspect ratio for its definition of the ratio of the wing span squared to wing area and cleaning up the equation results in:

$$\frac{L}{D} = \frac{W_o}{\frac{1}{2} \rho V^2 S C_{D_o} + \frac{2}{\rho \pi e} \left(\frac{W_o}{b} \right)^2 \frac{1}{V^2}} \quad (3.16)$$

Equation (3.16) defines the maximum aerodynamic performance possible for an aircraft with a given wing span, wing area, Oswald efficiency factor, and gross weight. A base drag coefficient or a desired maximum L/D can be defined to compute the drag polar.

3.2. Flight Envelope Formulation

The flight envelope is derived by equating (3.9) and (3.16) to each other and solving for velocity.

$$\begin{aligned} \frac{L}{D} &= \frac{VE}{\eta_p \eta_{em}} \frac{1}{\eta_{bat} \epsilon_{bat} x \beta + \eta_{gt} \eta_{gen} \epsilon_{gas} \ln \left(\frac{1}{1 - (1-x)\beta} \right)} \\ &= \frac{W_o}{\frac{1}{2} \rho V^2 S C_{D_o} + \frac{2}{\rho \pi e} \left(\frac{W_o}{b} \right)^2 \frac{1}{V^2}} \end{aligned} \quad (3.17)$$

For simplicity, a temporary variable (σ) will be used to define the specific energy and energy weight fraction blending term:

$$\sigma = \eta_{bat} \epsilon_{bat} x \beta + \eta_{gt} \eta_{gen} \epsilon_{gas} \ln \left(\frac{1}{1 - (1-x)\beta} \right) \quad (3.18)$$

Which simplifies Equation (3.17) to:

$$\frac{L}{D} = \frac{VE}{\eta_p \eta_{em}} \frac{1}{\sigma} = \frac{W_o}{\frac{1}{2} \rho V^2 S C_{D_o} + \frac{2}{\rho \pi e} \left(\frac{W_o}{b} \right)^2 \frac{1}{V^2}} \quad (3.19)$$

The following steps are taken in an attempt to isolate velocity:

$$\frac{VE}{\eta_p \eta_{em}} \left(\frac{1}{2} \rho V^2 S C_{D_o} + \frac{2}{\rho \pi e} \left(\frac{W_o}{b} \right)^2 \frac{1}{V^2} \right) = W_o \sigma \quad (3.20)$$

$$\frac{1}{2} \rho V^2 S C_{D_o} + \frac{2}{\rho \pi e} \left(\frac{W_o}{b} \right)^2 \frac{1}{V^2} = \frac{W_o \sigma \eta_p \eta_{em}}{VE} \quad (3.21)$$

$$\frac{1}{2} \rho V^2 S C_{D_o} - \frac{W_o \sigma \eta_p \eta_{em}}{VE} + \frac{2}{\rho \pi e} \left(\frac{W_o}{b} \right)^2 \frac{1}{V^2} = 0 \quad (3.22)$$

$$\left(\frac{1}{2} \rho S C_{D_o} \right) V^4 - \left(\frac{W_o \sigma \eta_p \eta_{em}}{E} \right) V + \frac{2}{\rho \pi e} \left(\frac{W_o}{b} \right)^2 = 0 \quad (3.23)$$

The equation is now conforming to a quartic function. Finding the roots of Equation (3.23) will produce four solutions: maximum velocity, minimum velocity, and two imaginary

numbers.

Maximum and minimum velocity for a given serial hybrid aircraft can be computed using Equation (3.23). To capture the entire flight envelope and answer the question of how fast and how high the aircraft can fly for a specified endurance, altitude will need to be varied starting at sea level conditions and Equation (3.23) will need to be recomputed increasing in altitude until the quartic function no longer provides real roots.

When finding the maximum altitude and associated airspeeds, Equation (3.23) assumes that the flight envelope is purely theoretical and does not account for any air breathing component, such as the gasoline engine in the hybrid cases. An assumption is also made that this envelope encompasses aerodynamic capabilities based on the net available energy onboard and does not account for stall speed or structural limitations. The flight envelope also does not factor in human physiology or air traffic control concerns. A lift coefficient overlay and a Mach overlay can be added to the flight envelope for reference.

3.3. Electric Motor Efficiency Map

Electric motor efficiency can be determined from either test data, manufacturer data, or a physics based model. The methods used here assume that the electric motor efficiency map is provided by the manufacturer. Many manufacturers already provide this data and can be found in the public domain. A few examples of manufacturer provided efficiency maps include, but is not limited to, YASA Motors, Remy International, Inc., GKN, and UQM Technologies. If a motor controller (inverter) is required, the efficiency of this process is also often included in the motor efficiency map. It is important to note that the electric motor efficiency must be defined in terms of torque and RPM. This format

would then be compatible with the propeller efficiency and noise format for comparison mapping that will be developed in the following sections. The YASA-750 motor map of torque versus RPM provided by the manufacturer is shown in Figure 3.1.

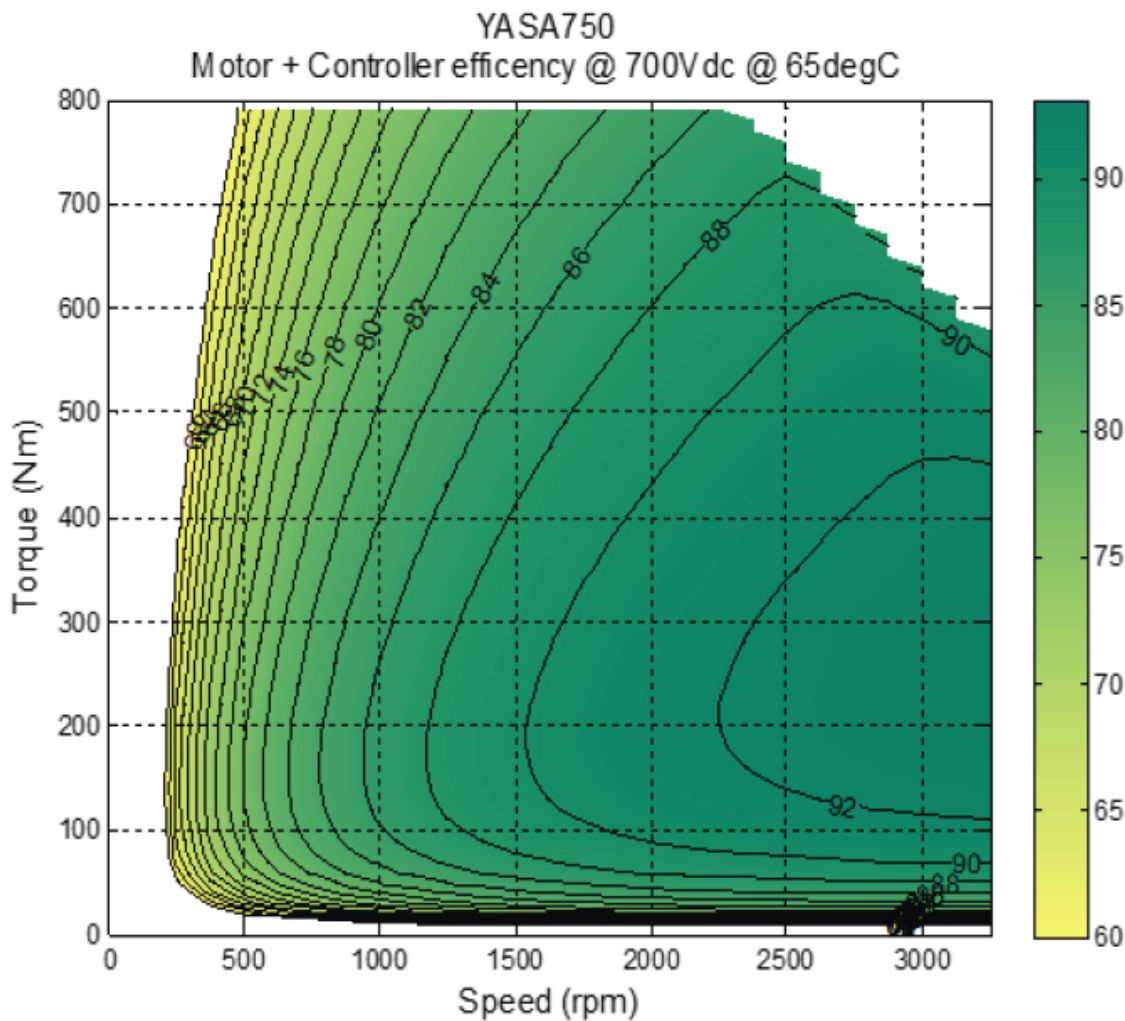


Figure 3.1. YASA-750 motor and controller net efficiency

It is important to note that this map was generated at a specific operating voltage of 700 volts. Electric motors can also be provided with maximum power and torque curves based on a given operating voltage. This too was provided by YASA Motors and is shown in Figure 3.2.

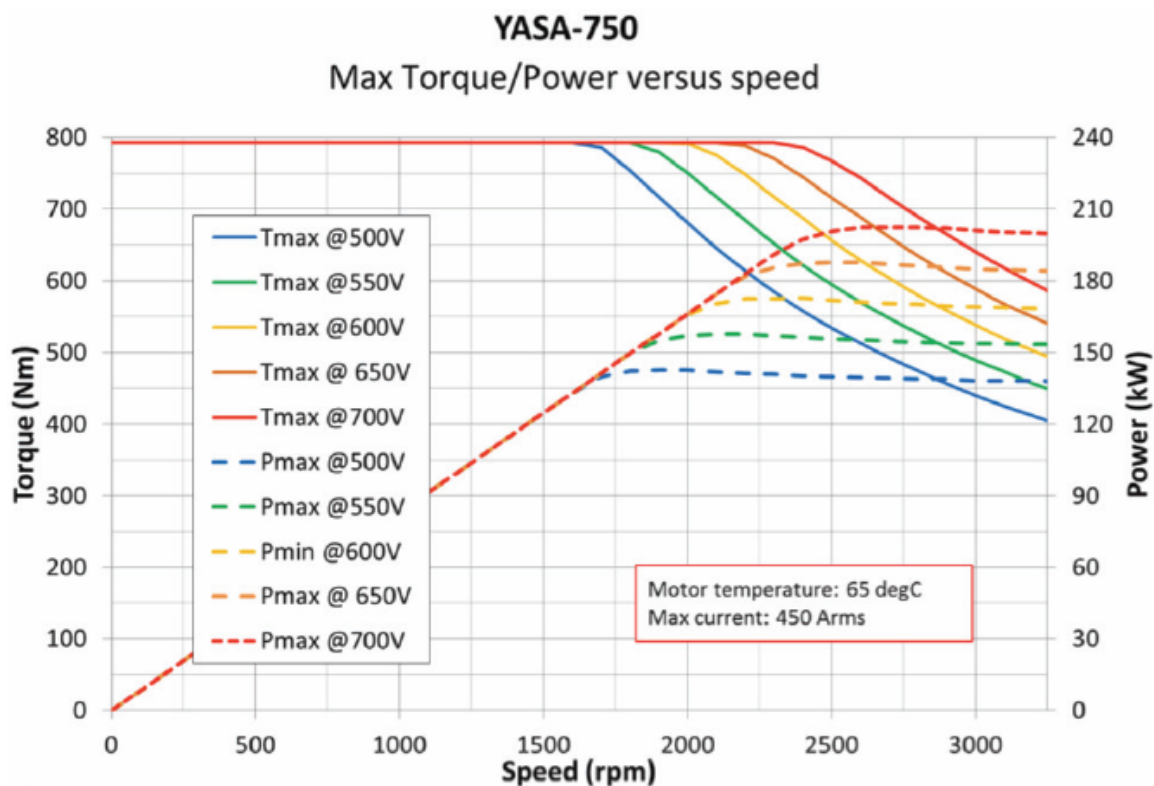


Figure 3.2. Maximum power and torque versus RPM

The curves shown in Figure 3.2 represent operating capability at various voltages in terms of both maximum torque and maximum power. The solid red (uppermost) curve represents the maximum torque that is represented in Figure 3.1 where the efficiency map appears to be jagged and cuts off. Since the maximum torque and power is denoted for voltages ranging from 500 volts to 700 volts, the efficiency map in Figure 3.1 is assumed to be applied over this voltage range for this particular motor since the only other efficiency data available is for an operating voltage of 400 volts or less.

The data is acquired from the electric motor efficiency map using a plot digitizing tool. Figure 3.1 is digitized using points along a single efficiency contour and saving the torque and RPM data points to a spreadsheet. This process is repeated for all of the

efficiency contours on the map. While a map can be generated from this data, it does not include any of the data in between the defined curves. An interpolation scheme was then coded using MATLAB® to read the data from various contours and interpolate between them to populate a torque versus RPM efficiency database. Both linear and cubic spline interpolations are used to help smooth out the data as needed.

3.4. Propeller Efficiency Map Formulation

The propeller efficiency map is the next step in the process for determining the net propulsive efficiency. Propeller efficiency can either be determined from theory or given in the manufacturer provided data. In either case, the efficiency must be defined as a grid in terms of advance ratio and coefficient of power for the following method to work. The ultimate goal is to be able to generate a propeller efficiency map on a torque versus RPM grid so it is compatible with the electric motor map. EFRC has an MTV-1-A/184-51 propeller manufactured by MT-Propeller with manufacturer provided efficiency data with respect to advance ratio and coefficient of power. This propeller data is used in developing the efficiency map in terms of torque versus RPM.

The torque and RPM ranges should be defined based on the same values that are used in the electric motor map. Taking the product of these two inputs results in propeller power:

$$P = Q \cdot RPM \quad (3.24)$$

The result of Equation (3.24) is then be plugged into Equation (2.3) to compute the coefficient of power at a specified altitude and airspeed. The advance ratio is computed using Equation (2.2). From here, the resulting efficiency is found from the manufacturer

provided data employing interpolation as needed.

Once this process is completed for all applicable torque and RPM combinations, a propeller map is plotted for a fixed altitude and airspeed. However, since the data is bounded by a maximum and minimum advance ratio and coefficient of power, several combinations of torque and RPM require efficiency extrapolation. While extrapolation can be achieved, there is still a defined propeller bound where the data is either given or interpolated. To define this bound, start by computing the maximum and minimum RPM possible for a given maximum and minimum advance ratio. Solving Equation (2.2) for RPM yields:

$$RPM_{min} = \frac{V}{J_{max}D_p} \cdot 60 \quad (3.25)$$

$$RPM_{max} = \frac{V}{J_{min}D_p} \cdot 60 \quad (3.26)$$

A conversion factor is included to convert revolutions per second to RPM. Since equations (3.25) and (3.26) are not a function of torque, they define the absolute maximum and minimum RPM that will produce an advance ratio that is within the provided data range. Coefficient of power bounds now need to be defined by calculating the maximum and minimum torque for a given maximum and minimum coefficient of power. Solving Equation (2.3) for torque while applying Equation (3.24) results in:

$$Q_{min} = C_{P_{min}} \frac{\rho n^3 D_p^5}{RPM} \quad (3.27)$$

$$Q_{max} = C_{P_{max}} \frac{\rho n^3 D_p^5}{RPM} \quad (3.28)$$

Equations (3.27) and (3.28) are a function of RPM as well. In order to plot the entire bound, maximum and minimum torque need to be computed for all applicable RPMs that are used in finding the propeller efficiency. The propeller efficiency map can now be developed for a given altitude and airspeed, with or without extrapolation, and a defined propeller bound to show where the data is true versus extrapolated.

It is also desirable to show curves of constant thrust on this propeller efficiency map. Thrust needs to be defined as a function of torque and RPM to be compatible. The derivation for this equation will start with a form of Equation (2.6), repeated below, for convenience:

$$\eta_p = \frac{TV}{P} \quad (3.29)$$

Substitute Equation (3.24) in for power:

$$\eta_p = \frac{TV}{Q \cdot RPM} \quad (3.30)$$

Solving for torque produces the final result:

$$Q = \frac{TV}{\eta_p \cdot RPM} \quad (3.31)$$

Similar to the propeller bound, Equation (3.31) needs to be computed for all applicable RPMs. Propeller efficiency is assumed to be equal to one (1) when computing Equation (3.31) since the propeller efficiency map is given. The thrust curve behaves as an overlay to demonstrate how efficient the propeller is at a given constant thrust. The efficiency is not constant and does not necessarily have a relationship to torque or RPM at any constant thrust value.

3.5. Propeller Noise Map Modeling

Modeling aircraft noise is not trivial. In classical aircraft with gasoline engines, both the propeller and engine generate noise. At lower operating engine speeds, the engine dominates the noise output. At higher operating speeds, the propeller will begin to dominate the perceived noise levels. Hybrid and electric aircraft making use of an electric motor and controllable-pitch propeller primarily only have propeller noise considerations. The electric motor is virtually silent in comparison to the propeller for all operating speeds. This reduces the noise problem to only one component, the propeller, which can be altered to vary the noise footprint on the ground.

The noise from the propeller at some position from the propeller is a function of its rotational speed, blade pitch (which produces a specific torque), true airspeed, distance from the propeller and position relative to the rotational axis of the propeller. The total magnitude of the noise generated by a propeller at constant thrust could be generalized by high noise at high rotational speeds due to sonic tip speeds. High noise can also be generated by reducing rotational speed at constant thrust yielding blade pitch angle that produce separation (stall). Between these two extremes is a noise minimum. It can be seen in Figure 3.3 that noise is a function of rotational speed and blade angle.

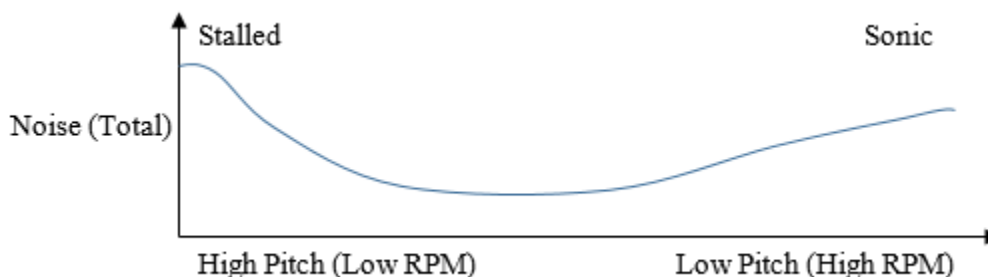


Figure 3.3. Noise at constant thrust

The noise, however, does not radiate out equally as a point source. The noise from a propeller is directional. As a result, there are directions that are noisier than others. The direction of maximum noise is a function of true airspeed, rotational speed, and blade angle. Define the azimuth angle (δ) from the rotational axis of the propeller forward as zero (0) degrees and proceeding to 90 degrees, the propeller disk plane.

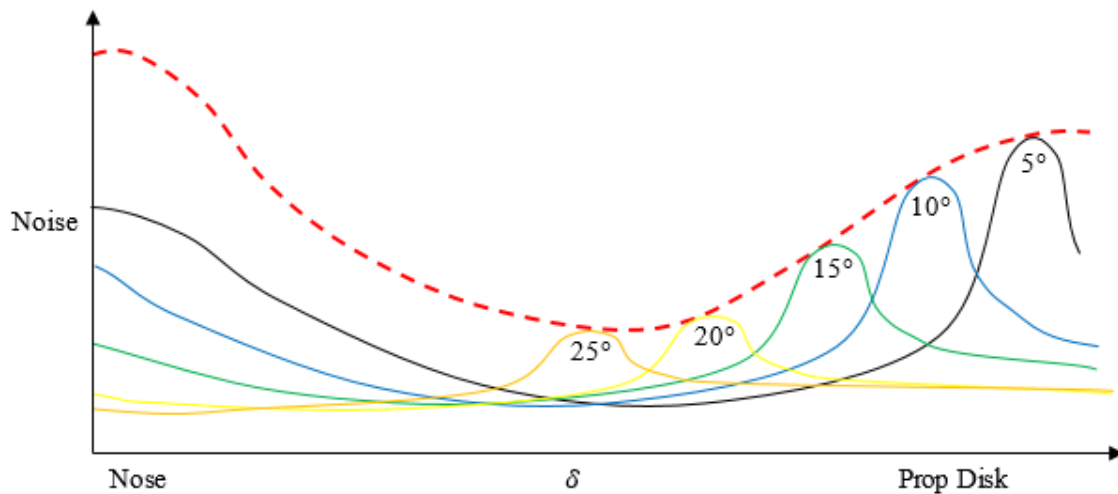


Figure 3.4. Noise at constant thrust based on blade pitch angle

With the combination of a controllable-pitch electric propeller and an electric propulsive motor, constant thrust can be maintained while using blade pitch to reposition the point of maximum noise.

It is imperative to be able to compute the noise based on a given methodology that only requires basic propeller geometry and high level flight conditions. The Hamilton Standard method does this task exactly and is used to generate arbitrary propeller noise maps.

Table 3.1. Hamilton Standard far-field propeller noise prediction inputs

Parameter		Units
Propeller diameter		ft
Number of blades per propeller		-
Number of propellers		-
Rotational speed		RPM
Power input per propeller		shp
Location, relative to the propeller(s), of the point at which the noise is to be defined	Distance	ft
	Azimuth	deg
Flight speed		KTAS
Ambient temperature		°F

The method consists of determining a series of partial levels and correction factors that are summed arithmetically to make a propeller noise prediction. The partial levels and correction factors come from figures and data tables that were derived based on available propeller noise test data. The estimation is therefore restricted to having a data point on these figures without extrapolation.

A MATLAB® code is written to generate a propeller noise map in terms of torque and RPM. This is done so the noise can directly overlay with the propeller and electric motor efficiency to visually quantify how much noise the propeller makes with respect to efficiency at a given thrust or power setting. In this setting, power input per propeller is arbitrary due to the nature of the torque versus RPM map.

3.6. Geographical Considerations for Noise Mitigation

A map of noise pertinent variables such as propeller rotational speed, blade pitch, angle of attack, and true airspeed can be generated for each propulsion system. Similarly, a map of noise sensitive areas could be generated on the surface of the Earth in terms of latitude, longitude, and a noise sensitivity index (NSI).

3.6.1. Noise Directivity

Recall that propeller noise does not radiate out equally as a point source. This is directionally dependent for which there are azimuths that are noisier than others. With a map of noise directionality and a map of noise sensitive areas in a North-East-Down (NED) system, ground noise could be predicted through the attitude (Euler angles) and the position of the aircraft from an inertial measurement unit (IMU) or global positioning system (GPS).

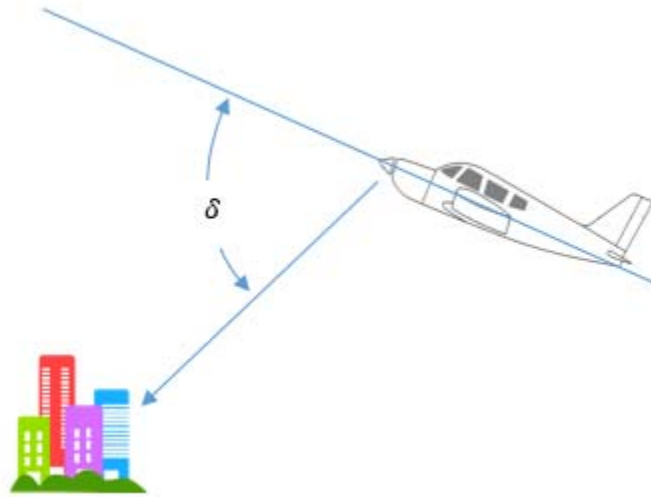


Figure 3.5. Noise directivity

Using the anticipated flight path of the aircraft, the noise could be mitigated through noise sensitive areas by changing the blade pitch and RPM while maintaining constant thrust. An optimization algorithm could be used knowing the noise map, geographical map, and state vector of the aircraft. The maximum noise position of the aircraft could be moved rapidly or jumped across noise sensitive areas and left to linger in non-sensitive areas.

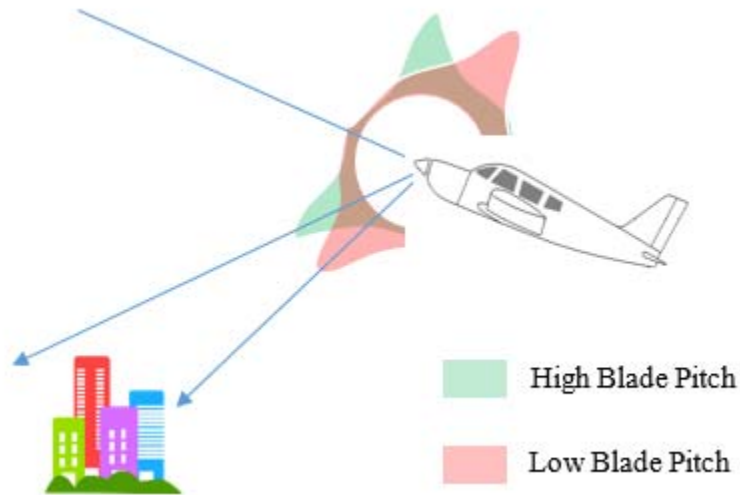


Figure 3.6. How the position of maximum noise can move at constant thrust

The combination of an electric motor and controllable-pitch propeller can minimize noise in noise sensitive areas while not compromising the performance of the aircraft.

3.6.2. Noise Distance and Azimuth Angle Computation

Perceived noise is a function of the distance from the propeller and azimuth angle relative to the propeller axis in the forward direction. It is desired to be able to define the distance and azimuth based on the aircraft's position and attitude with respect to an observer or measurement device on the ground. Position is defined in terms of latitude, longitude, and altitude, while the attitude is defined as pitch angle, bank angle, and heading. The bank angle is assumed to rotate about the aircraft's longitudinal axis. The propeller axis is assumed to be in the same direction as the aircraft's longitudinal axis.

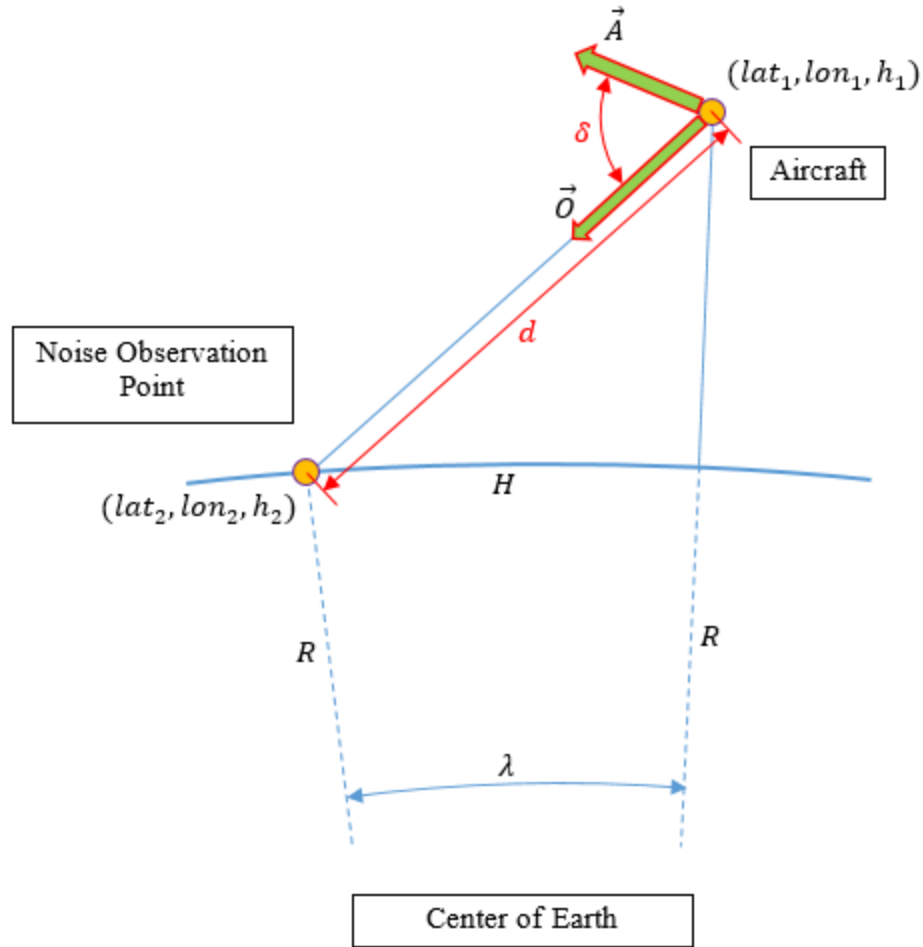


Figure 3.7. Representation of noise distance and azimuth

The distance or arc length (H) between a pair of latitudes and longitudes is easily computed using the Haversine formula and assuming a round Earth (Gleyzer, 2017):

$$f = \sin^2\left(\frac{lat_2 - lat_1}{2}\right) + \cos(lat_1)\cos(lat_2)\sin^2\left(\frac{lon_2 - lon_1}{2}\right) \quad (3.32)$$

$$g = \text{atan2}(\sqrt{f}, \sqrt{1-f}) \quad (3.33)$$

$$H = 2R \cdot g \quad (3.34)$$

The distance defined does not yet account for altitude difference between the aircraft and an observer. Using the law of cosines, the net distance (d) between the aircraft and observer positions can be computed as follows:

$$\lambda = \frac{H}{R} \frac{360}{2\pi} \quad (3.35)$$

$$d = \sqrt{(R + h_1)^2 + (R + h_2)^2 - 2(R + h_1)(R + h_2)\cos(\lambda)} \quad (3.36)$$

The azimuth angle must now be computed to complete the function. Using the aircraft position as the origin, two 3D vectors can be drawn, one pointing towards the observer (\vec{O}) and the other in the direction of the aircraft's longitudinal axis (\vec{A}). The angle between these vectors is the azimuth angle and is computed as follows:

$$\delta = \arccos\left(\frac{\vec{O} \cdot \vec{A}}{\|\vec{O}\| \|\vec{A}\|}\right) \quad (3.37)$$

Where:

$$\vec{O} = \langle dlat, dlon, dh \rangle \quad (3.38)$$

$$\vec{A} = \langle \cos(\theta)\cos(\psi), \cos(\theta)\sin(\psi), \sin(\theta) \rangle \quad (3.39)$$

The latitude and longitude terms within \vec{O} are computed using the Haversine formula without any altitude correction since the goal is to define component vectors in NED. The first term in each vector represents the 'North' component, the second term 'East', and the third term 'Down'. To compute $dlat$, a constant longitude is applied to the Haversine formula to find the distance between the two latitude lines. To compute $dlon$, a constant latitude is applied to the Haversine formula to find the distance between the two longitude

lines. Finally, to compute dh , the observer's altitude is subtracted from the aircraft's altitude. If the aircraft is north or east of the observer, a negative correction factor is required to compute the correct azimuth angle. If the aircraft is north of the observer, $dlat = -dlat$, and if the aircraft is east of the observer, $dlon = -dlon$. This correction only applies if the variable assignment shown in Figure 3.7 is used where position one (1) is the aircraft and position two (2) is the observer.

3.6.3. Noise Sensitivity Index

The NSI is rated on a scale of one (1) to ten (10) where one (1) is defined as the least sensitive and ten (10) is the most sensitive to noise. This index comes into play when defining noise sensitive areas over the Earth. For example, the ocean would likely find a NSI of one (1), while a major city would likely have a sensitivity index of ten (10). This index couples with position defined in latitude and longitude. A map can be drawn in a similar fashion to that of an aeronautical sectional chart, however, instead of defining airspace, noise sensitivity zones can be represented.

3.7. Flight Envelope Overlay

Efficiency and noise are overlaid onto the flight envelope as means of viewing the big picture of the serial hybrid aircraft performance: how high, how fast, how efficient, and how much noise. Both efficiency and noise maps are computed at a given altitude and airspeed using the methods outlined in Sections 3.3 through 3.6. By choosing a torque and RPM combination at a specified thrust or power setting, a single value of efficiency and noise is determined at the given altitude and airspeed. The specific torque and RPM combination used can also be tied to the NSI to maximize efficiency, minimize noise, or

choose an operating point in between. The efficiency and noise maps need to be recreated for every altitude and airspeed within the flight envelope to create the final contour overlay. If the flight envelope is large, incremental values in a gridded fashion can be used to vary altitude and airspeed combinations.

4. Analysis and Results

The EFRC's Diamond HK-36 aircraft will be used for the primary analysis and baseline configuration. While the aircraft is intended to be a fully electric aircraft, serial hybrid configurations will be analyzed as well to be able to compare battery improvements, aircraft hybridization, and aerodynamics. The HK-36 is also retrofitted with a YASA-750 motor, a motor controller, and an electrically actuated controllable-pitch MT-Propeller. Therefore, these components are used to analyze efficiency and noise.

4.1. Design Space

Equations (3.9) and (3.16) are used to visualize the design space of a serial hybrid aircraft. In order to define the design space for the HK-36, several variables need to be numerically assigned in a baseline configuration. Note that several of the variables listed are subject to change or are not used in the fully electric case, however, they will be needed later on for performance comparison. The propeller and electric motor efficiencies are assumed to be equal to one (1) but will be modified later.

Table 4.1. Design space variable definitions based on the Diamond HK-36

Parameter	Variable	Value	Units
Maximum lift-to-drag ratio	L/D	28	-
Aircraft gross weight	W_o	1698	lbf
Wing area	S	165.7	ft ²
Wing span	b	53.58	ft
Oswald efficiency factor	e	0.7	-
Altitude	h	0	ft
Endurance	E	2	hr
Percent hybrid	x	1	-
Energy weight fraction	β	0.18	-
Battery specific energy (Sanyo 18650GA)	ϵ_{bat}	0.1533	hp-hr/lbf
Gas specific energy (100LL)	ϵ_{gas}	7.4345	hp-hr/lbf
Battery efficiency	η_{bat}	0.9	-
Electric motor efficiency	η_{em}	1	-
Gas turbine efficiency	η_{gt}	0.4	-
Generator efficiency	η_{gen}	0.8	-
Propeller efficiency	η_p	1	-

The design space for the fully electric HK-36 shown in Figure 4.1 includes multiple battery specific energies to demonstrate how performance improves as battery technology improves.

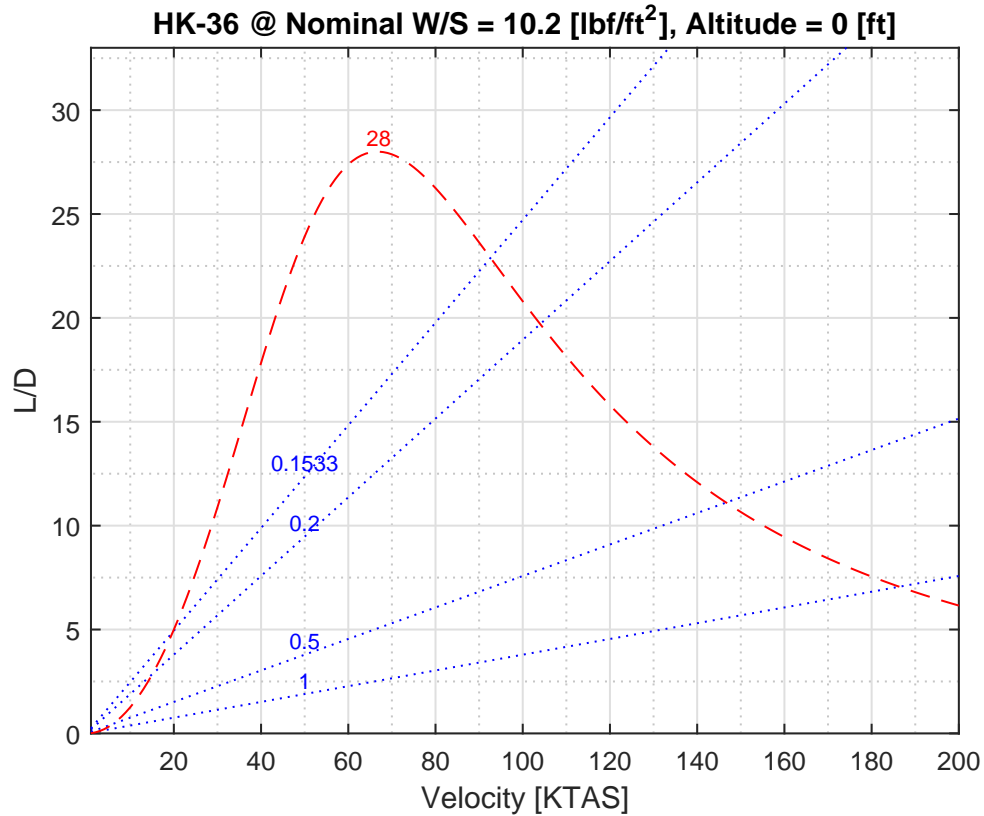


Figure 4.1. Diamond HK-36 100% hybrid design space

The interpretation of Figure 4.1 is that for the HK-36 to fly at the speed indicated with a battery specific energy designated on the blue line (short dashed line), a minimum aerodynamic efficiency (L/D) would be required. The area above the blue line (short dashed line) specifies an envelope of airspeed and L/D combinations that are possible from the net available energy standpoint. The area above the blue line (short dashed line) is limited by the red line (long dashed line) or drag polar. This yields an envelope that lies above the blue line (short dashed line) and below the red line (long dashed line). The intersection of these lines generates a minimum and maximum flight speed that is possible at a given altitude with a given battery specific energy. While the minimum airspeed is not of particular interest, a result of this analysis is a maximum airspeed for a given cruise

flight of a fully electric aircraft. It can be seen that as battery specific energy increases, the envelope expands significantly without changing any other parameters.

This same procedure can be followed for a theoretical hybrid case of the HK-36. Assume that the percent hybrid of the aircraft is now 90% instead of 100%. The design space displayed in Figure 4.2 drastically improves with a small quantity of fuel using the same energy weight fraction.

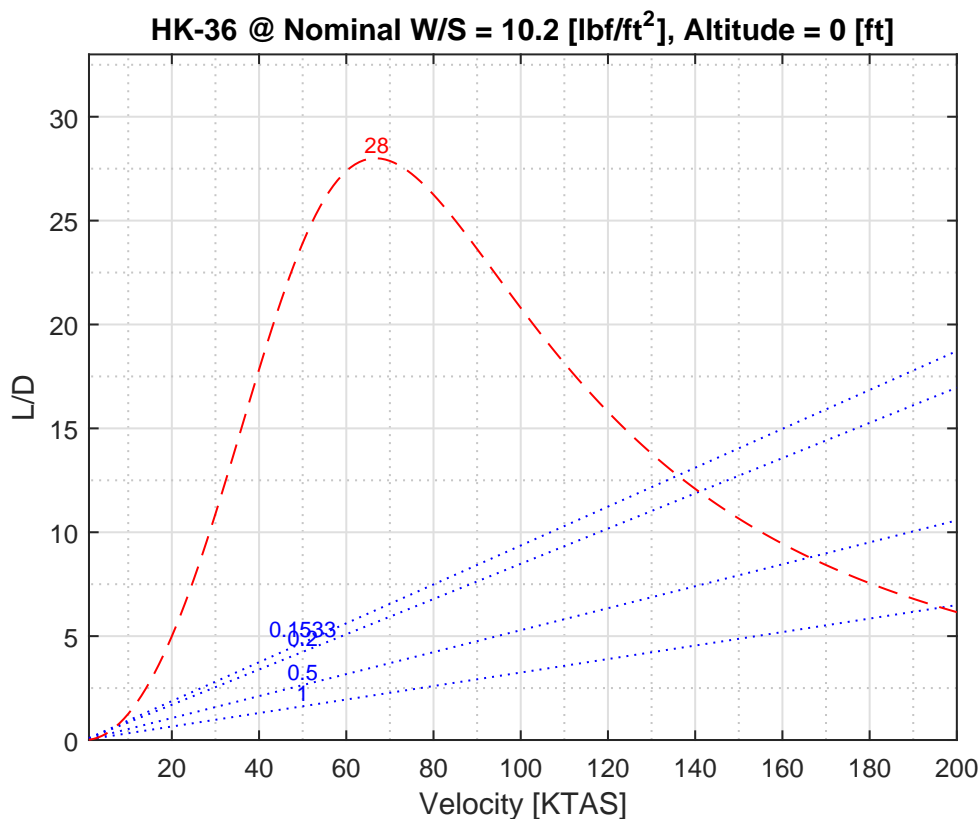


Figure 4.2. Diamond HK-36 90% hybrid design space

Comparing Figure 4.1 to Figure 4.2, the maximum airspeed for any battery specific energy is significantly faster for the 90% hybrid case. This analysis assumes that the fuel and electricity in the batteries are used simultaneously and can be combined through either a gearbox or electrically. Even with the high inefficiencies of using fuel, the net specific

energy available has a large weighing factor in terms of performance.

To truly appreciate how much the hybrid aircraft can outperform a fully electric one, the baseline battery specific energy is compared for both 100% hybrid (fully electric) and 90% hybrid cases as shown in Figure 4.3.

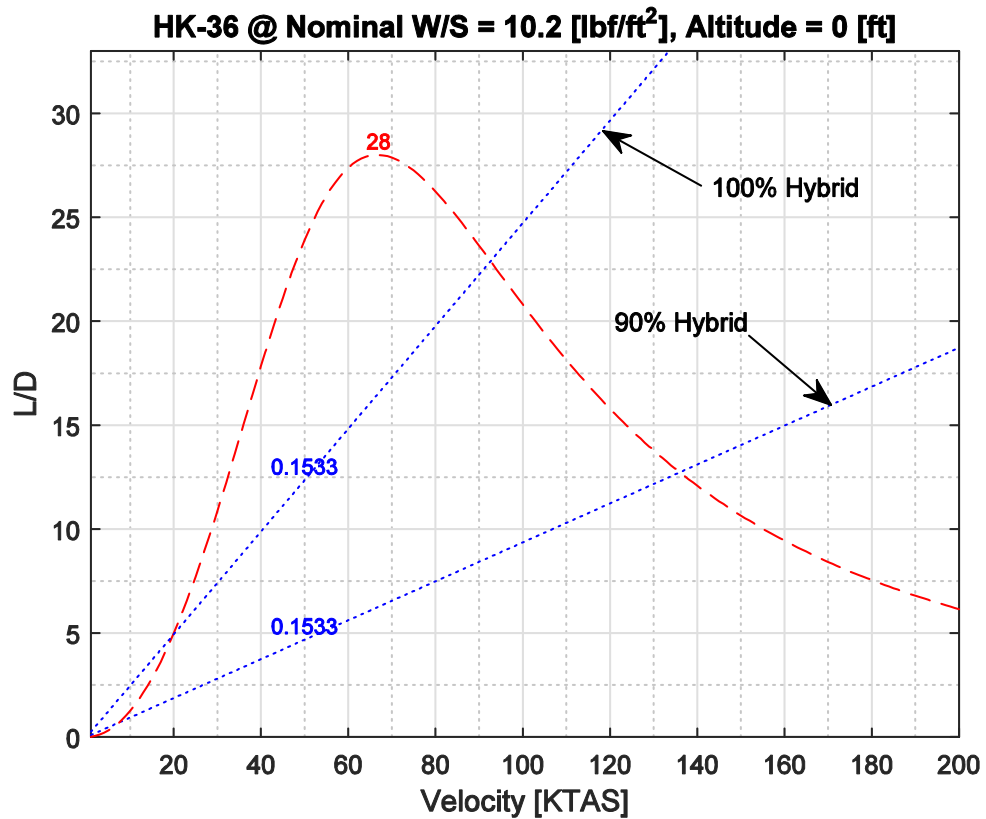


Figure 4.3. Diamond HK-36 100% to 90% hybrid comparison

Figure 4.3 indicates that the 90% hybrid HK-36 can fly nearly 50% faster without changing energy weight fraction or aerodynamics.

4.2. Flight Envelope

The design space demonstrates the envelope at which the HK-36 can fly with the parameters specified in Table 4.1. However, this approach only determines the envelope

for a single specific altitude. The flight envelope encompasses the entire set of altitudes and airspeeds at which the aircraft can sustain steady, level flight based on the inputs in Table 4.1. The envelope is determined using either a graphical approach or a computational approach. The graphical approach provides a visual intuition as to why there is a theoretical altitude and airspeed limitation on serial hybrid aircraft. However, the computational approach is significantly more practical to use when generating the envelope.

The graphical approach towards the flight envelope uses the HK-36 design space shown in Figure 4.4. In this case, the drag polar (long dashed line) is denoted by the altitude it was generated at while the entire figure assumes constant L/D . A second altitude of 30,000 ft is also included to show how the drag polar shifts to the right as altitude increases.

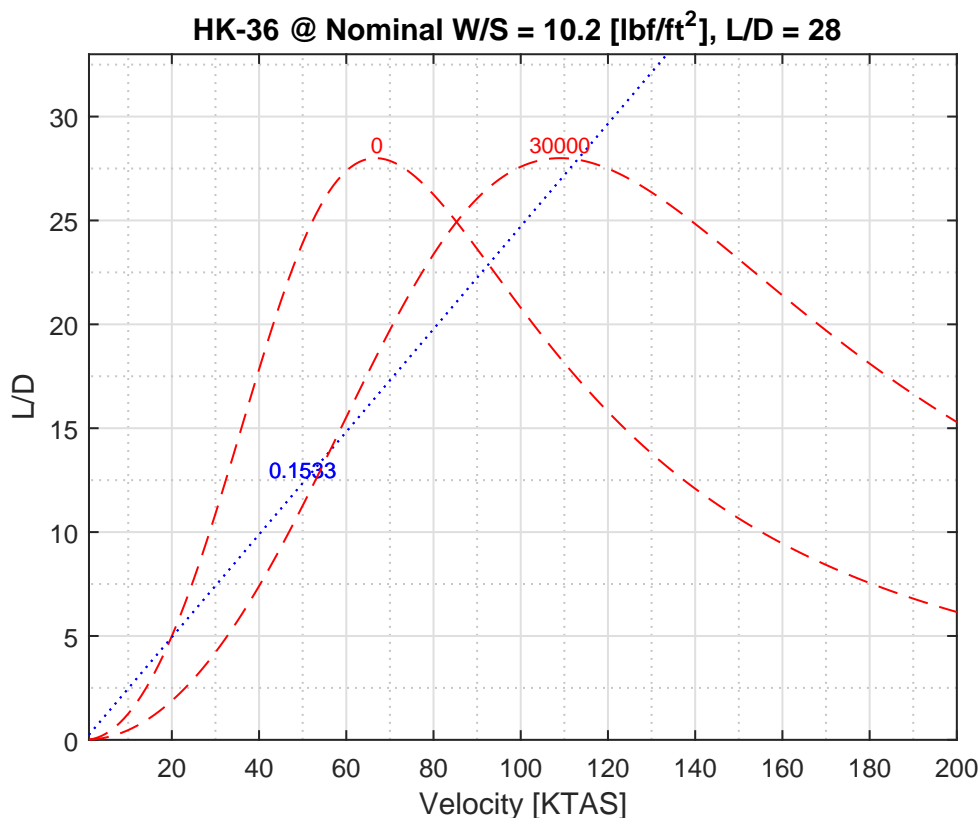


Figure 4.4. Diamond HK-36 100% hybrid design space

This shift is due to the increase in required power to operate at higher altitudes. As shown in Figure 4.4, both altitudes cross the blue line (short dashed line) at different maximum and minimum airspeeds. The flight envelope is a collection of these maximum and minimum velocities across incremental altitudes starting at sea level and increasing until the entire drag polar falls below the battery specific energy line. The airspeeds and altitudes collected generate the flight envelope shown in Figure 4.5.

The flight envelope computational approach uses Equation (3.23) and increases altitude starting from sea level until no real velocity satisfies the equation and all roots are imaginary. The result is the full spectrum of how fast and how high the aircraft can fly. The flight envelope shown in Figure 4.5 portrays that the HK-36 can fly for two (2) hours at any altitude and airspeed combination below the curve.

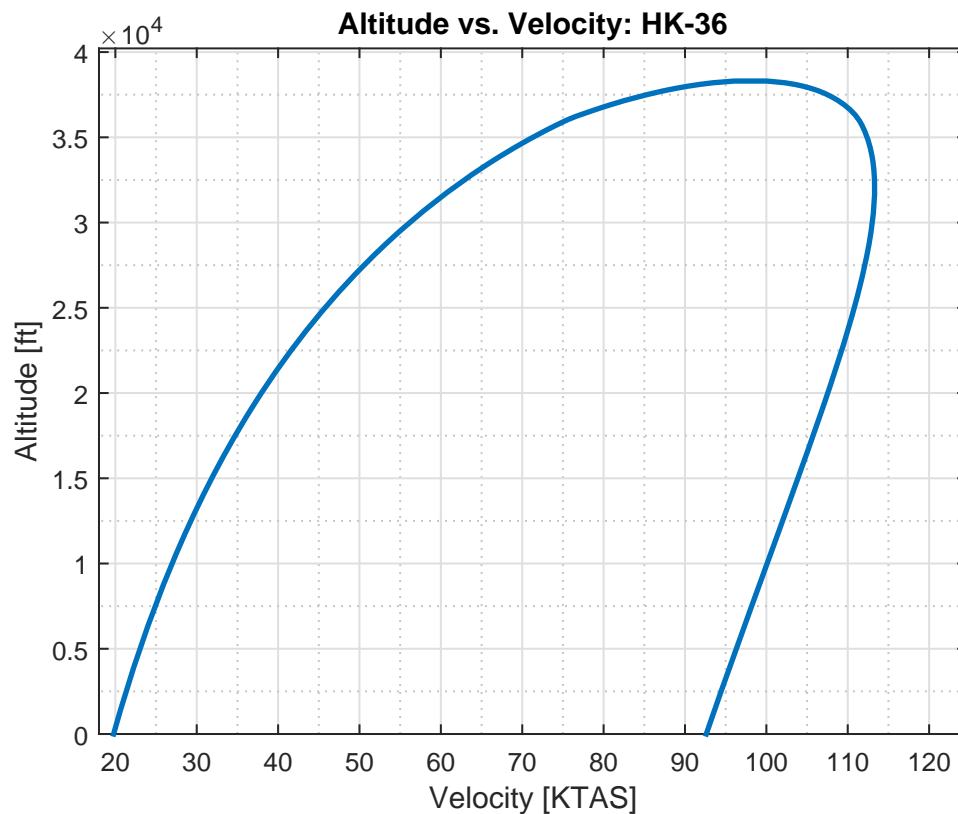


Figure 4.5. Diamond HK-36 100% hybrid flight envelope

Flight is achievable outside of the curve, however, a parameter or multiple parameters must be altered to reach the operating point. Figure 4.3 already demonstrates that a 90% hybrid aircraft can fly significantly faster without changing any other variables. The flight envelopes shown in Figure 4.6 compare the 90% hybrid case with the 100% hybrid case.

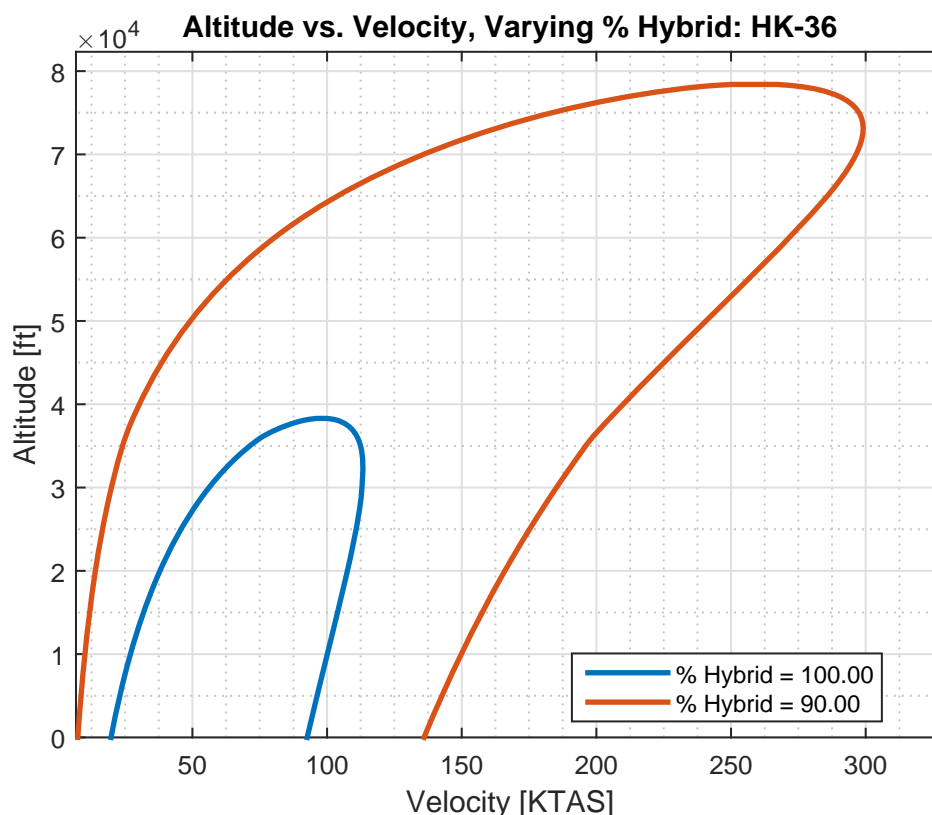


Figure 4.6. Diamond HK-36 100% and 90% hybrid flight envelope

The 90% hybrid case as shown in Figure 4.6 is capable of flying faster and higher than its 100% hybrid counterpart. This results in improved performance over fully electric with more available operating points.

The flight envelope can compare any of the parameters specified in Table 4.1 to each other. Multiple values can be used for a parameter to show how the flight envelope

changes while keeping the remaining variables constant. A few examples of this are provided by varying L/D , battery specific energy, and endurance separately from the baseline configuration.

Aerodynamics are an essential part to enabling hybrid and electric flight. As shown in Figure 4.7, improving aerodynamic efficiency significantly improves the flight envelope. In practice, aircraft cannot vary their aerodynamic performance in flight with respect to geometry and the airframe. However, an existing airframe that is converted to a hybrid aircraft may have its aerodynamics altered during the conversion process. Figure 4.7 demonstrates the effect of changing the base aerodynamics.

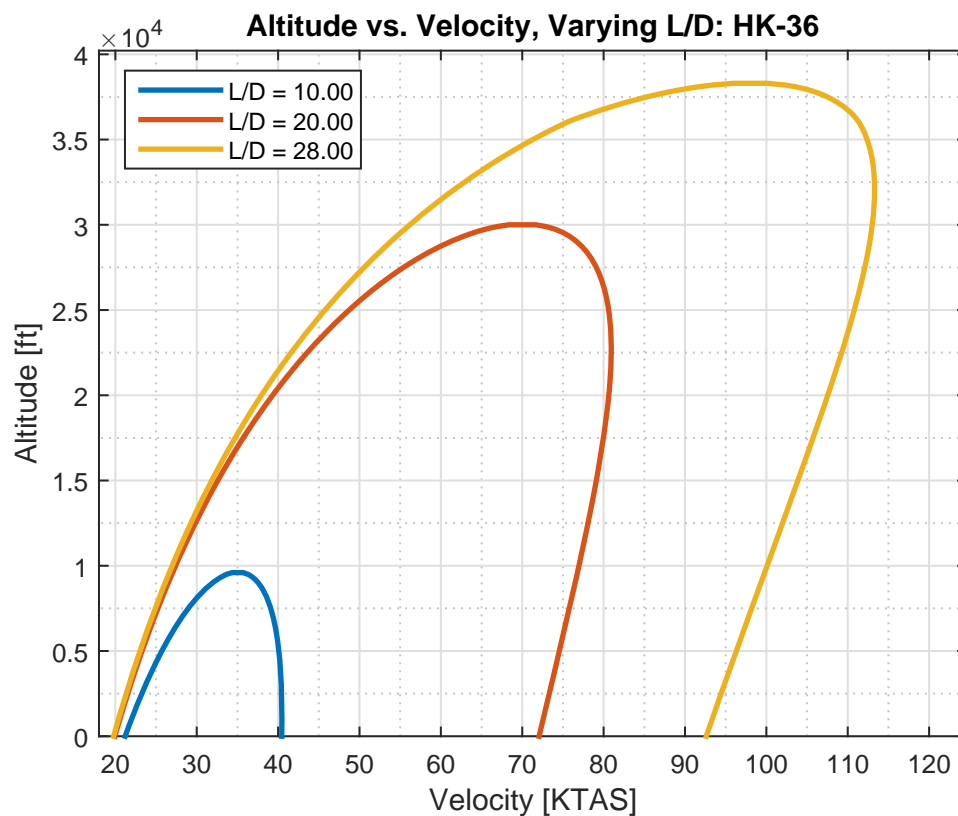


Figure 4.7. Diamond HK-36 varying aerodynamic efficiency flight envelope

Battery specific energy clearly has an impact on the flight envelope. As battery technology improves every year, so will the flight envelope, regardless of its hybridization. Battery centric aircraft use this benefit as long as the energy weight fraction remains constant. The same aircraft can fly faster and further theoretically every year assuming the same type of battery cell is used but with more energy packed into it.

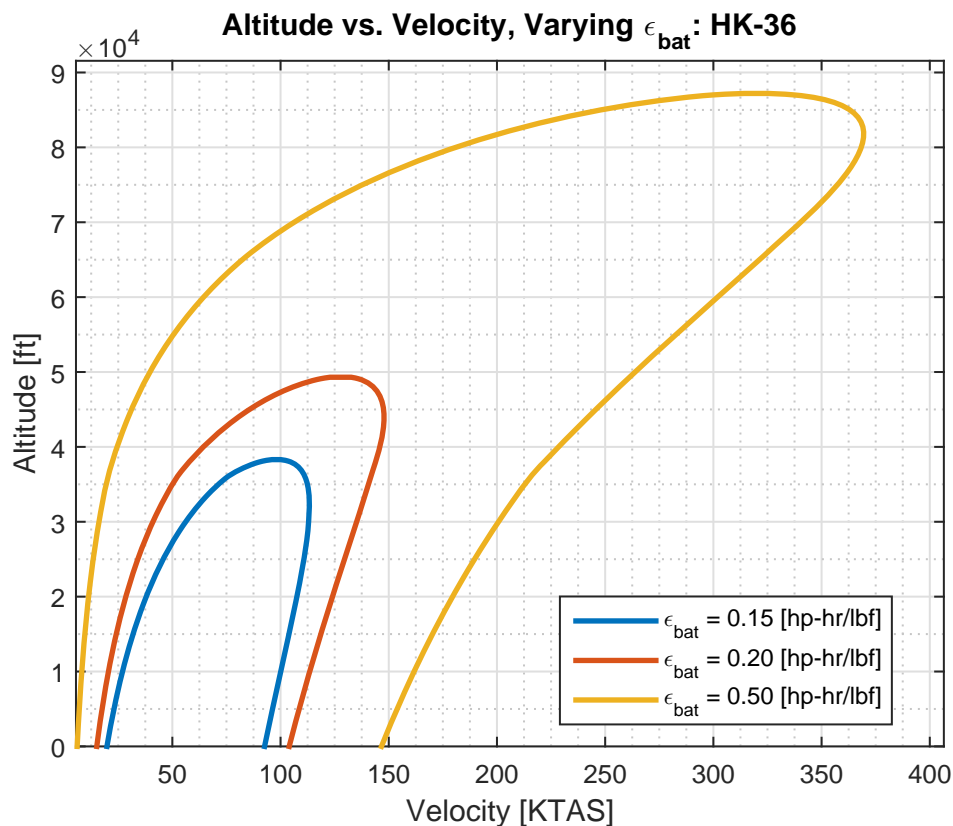


Figure 4.8. Diamond HK-36 varying battery specific energy flight envelope

Required endurance pays a large toll at the expense of performance. Figure 4.9 conveys that for a given aircraft, a shorter flight allows the pilot to fly faster and higher than a longer one. This can prove to be very useful when hybrid technology expands into longer haul flights.

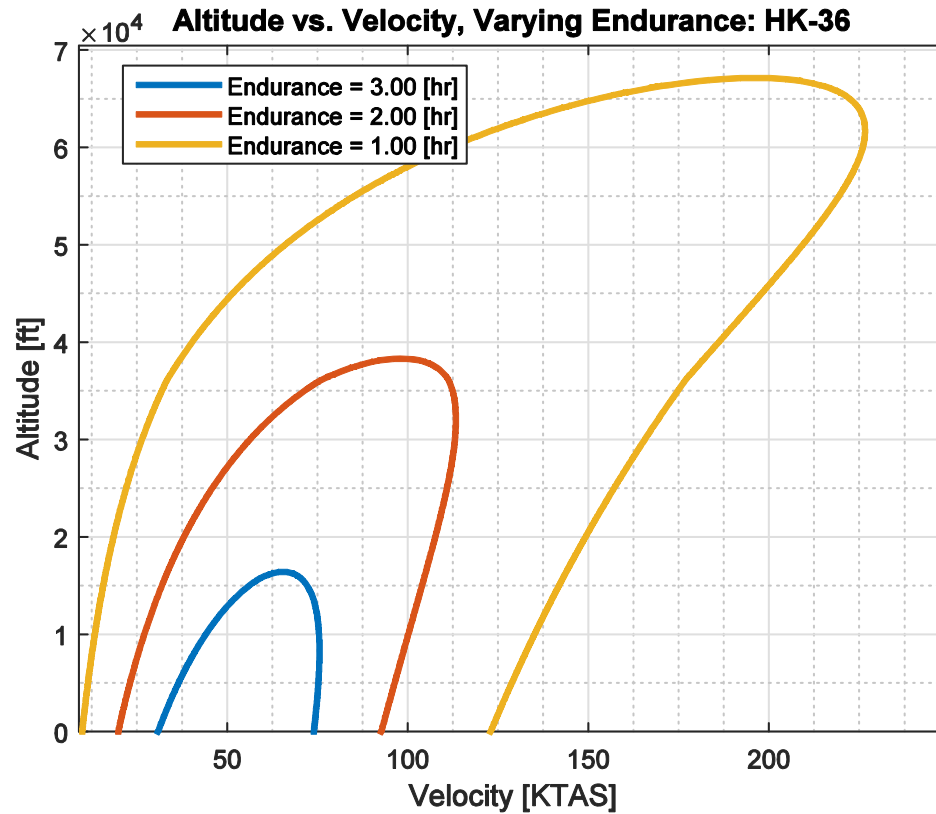


Figure 4.9. Diamond HK-36 varying endurance flight envelope

4.3. The Electric Motor and Propeller

Up to this point, electric motor and propeller efficiency has been assumed to be unity. The assumption was made due to the unique properties that this combination is capable of offering. Traditional gasoline engines have a fixed torque versus RPM curve meaning that it is impossible to operate without lying somewhere on the curve. An electric motor with an appropriate motor controller has the ability to vary torque and RPM independently. A controllable-pitch propeller exploits this feature and allows for operation at any torque and RPM combination with the ability to maintain constant thrust. The goal is to now be able to analyze efficiency and noise by using this fact.

4.3.1. Electric Motor Efficiency

The EFRC is currently using a YASA-750 motor for their HK-36. This motor is not only capable of producing nearly 100 hp, but it also much lighter and more compact than a gasoline engine of similar operating capabilities. YASA Motors provided the efficiency map for the motor as seen in Figure 3.1. This map was digitized and interpolated to regenerate the map in MATLAB® shown in Figure 4.10.

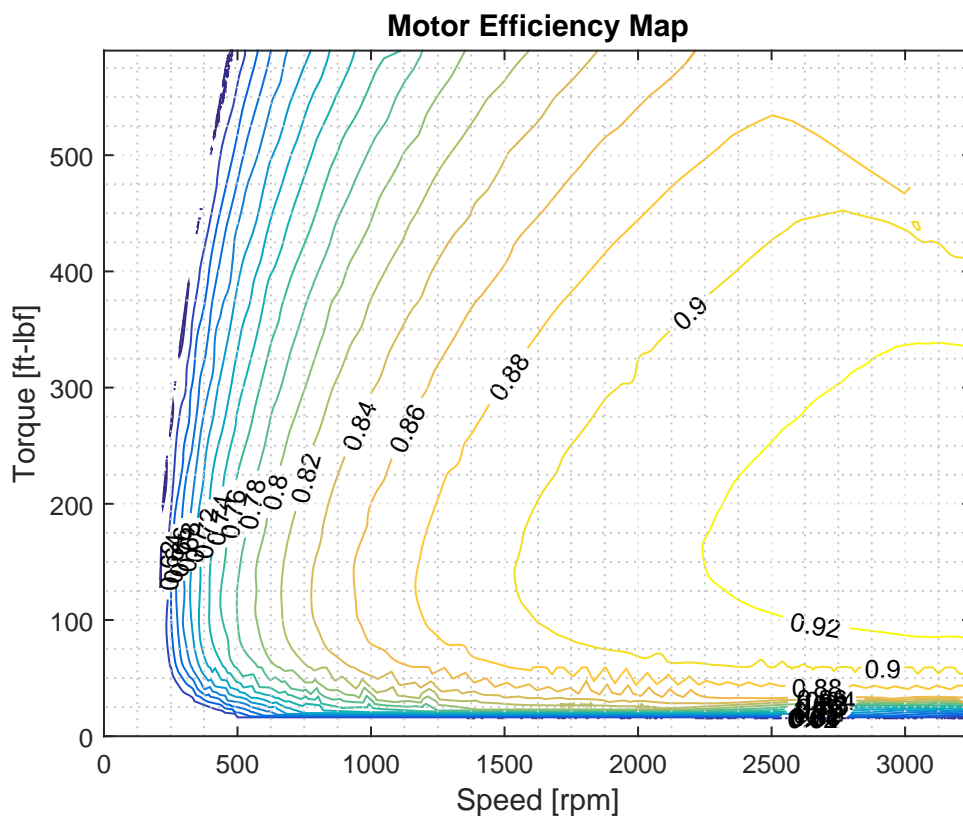


Figure 4.10. Digitized YASA-750 efficiency map

This map is assuming high voltage operation on an 800 volt system. The contours are not necessarily smooth in the low torque range due to the interpolation techniques used in MATLAB®, however, this will have very little impact on the primary result. It is also important to note that torque has been converted to English units in Figure 4.10 instead of

the given metric units shown in Figure 3.1.

The YASA-750 motor also has torque limitations with respect to RPM. The upper right hand corner of Figure 4.10 shows this by lacking efficiency data. Applying the maximum torque curves from Figure 3.2 and overlaying them onto the efficiency map provides limitations based on operating voltage.

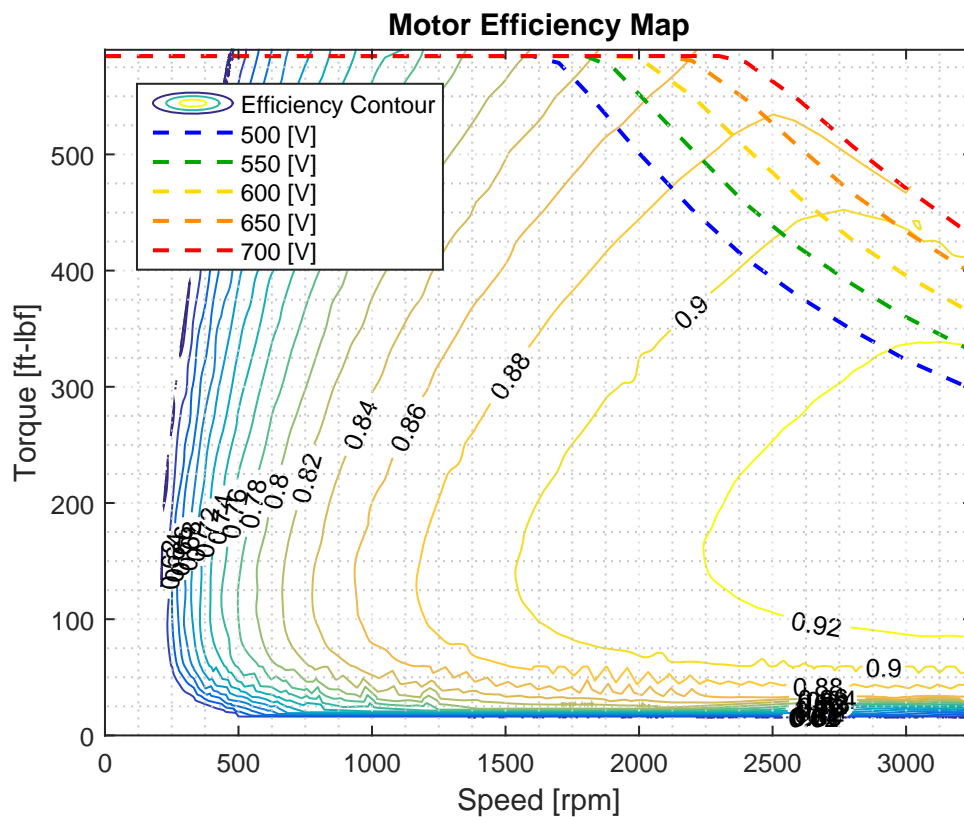


Figure 4.11. YASA-750 efficiency map with operating limitations

For simplicity, the motor will be assumed to be operating at 700 volts to clean up the additional voltage limitations for future figures.

4.3.2. Propeller Efficiency

The next step is to be able to map out propeller efficiency in a torque versus RPM grid so the data can be appropriately combined with the electric motor. The EFRC is using an electrically actuated controllable-pitch MT-Propeller. The propeller data provided is for the MTV-1-A/184-51 propeller in terms of advance ratio and coefficient of power. The data was provided by MT-Propeller in a table format and has been digitized to generate an efficiency map in MATLAB® as seen in Figure 4.12.

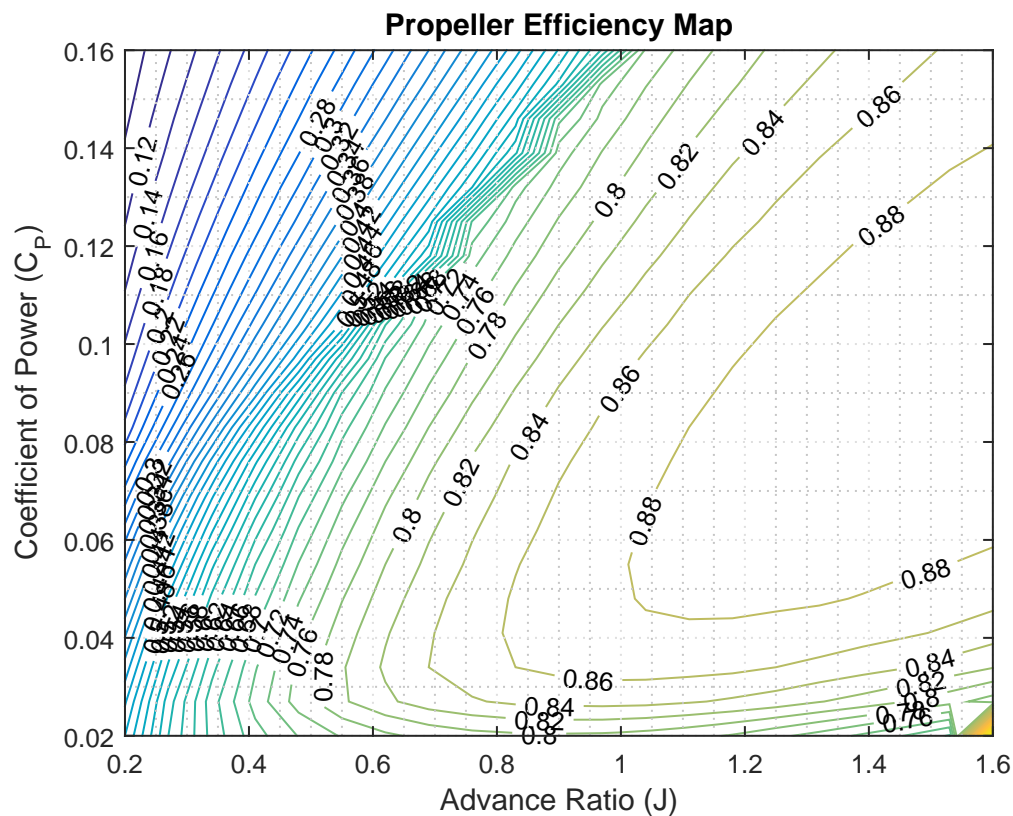


Figure 4.12. Digitized propeller efficiency map

The propeller efficiency map shown in Figure 4.12 is not comparable to the motor efficiency map due to the different axes. This is overcome by assuming an altitude and airspeed at which to analyze efficiency. Using the methodology in Section 3.4 allows

Figure 4.12 to be converted into a map with the same axes as the motor efficiency map as demonstrated in Figure 4.13. A few variables need to be defined to make the efficiency map. The Diamond HK-36 aircraft is assumed to be in a climb configuration so as to generate significant thrust.

Table 4.2. Propeller and aircraft variable definitions for efficiency

Parameter	Variable	Value	Units
Propeller diameter	D_p	6.04	ft
Aircraft velocity	V	59	KTAS
Altitude	h	500	ft
Propeller torque	Q	1 - 590	ft-lbf
Propeller RPM	RPM	1 - 3250	rpm

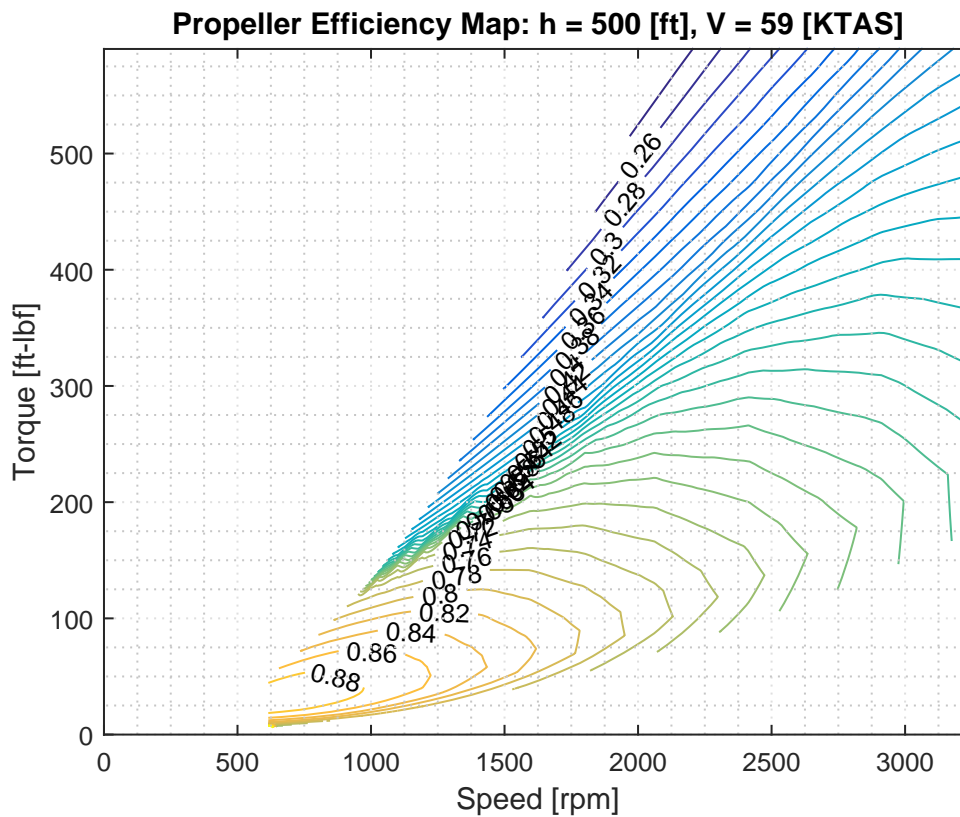


Figure 4.13. Propeller efficiency map

Similarly to the electric motor efficiency map, the propeller efficiency map also has operating constraints where the propeller data is either defined or requires extrapolation. The data provided has a maximum and minimum advance ratio and coefficient of power which creates a propeller bound for where the efficiency is defined. The bounds are computed using Equations (3.25), (3.26), (3.27), and (3.28) and are plotted with Figure 4.13 to generate Figure 4.14.

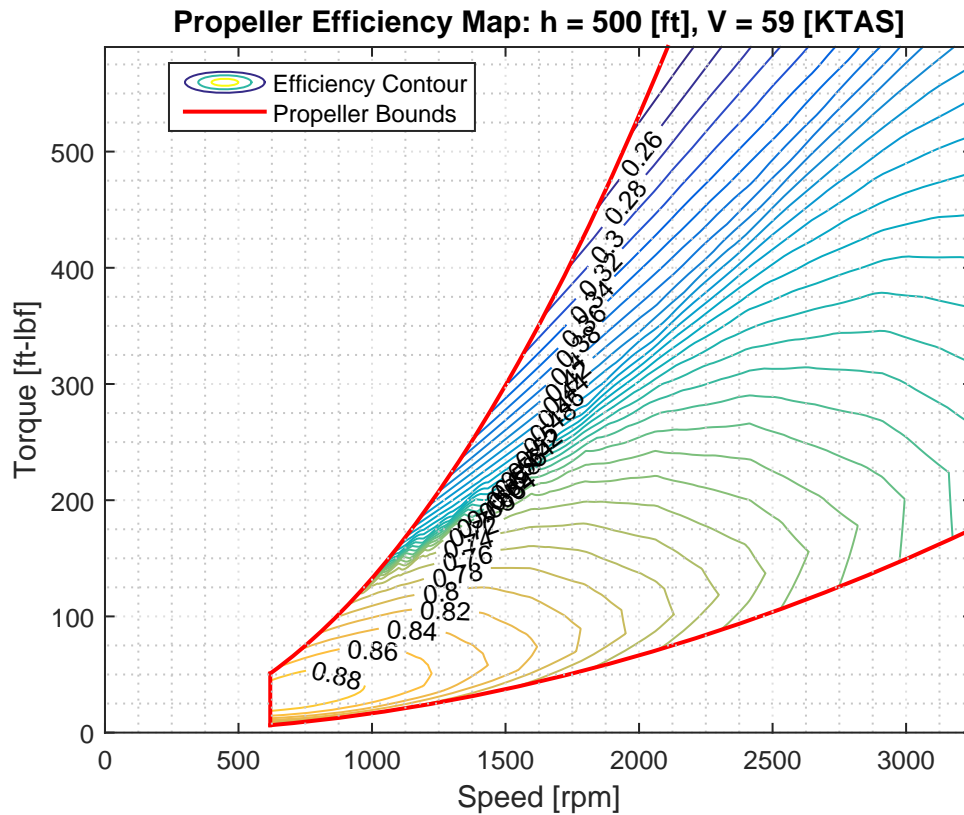


Figure 4.14. Propeller efficiency map with appropriate bounds

The efficiency map in Figure 4.14 is now limited to a given altitude and airspeed, however, it is actually more advantageous in this manner to be able to analyze different operating points in the flight envelope.

4.3.3. Combined Electric Motor and Propeller Efficiency

With both the electric motor and propeller efficiency maps now on the same axes and defined, they can be overlaid and combined into a single map including their operating limitations. The orange contours (contours bounded by the red dashed line) in Figure 4.15 represent the electric motor while the blue contours (contours bounded by the red solid line) represent the propeller.

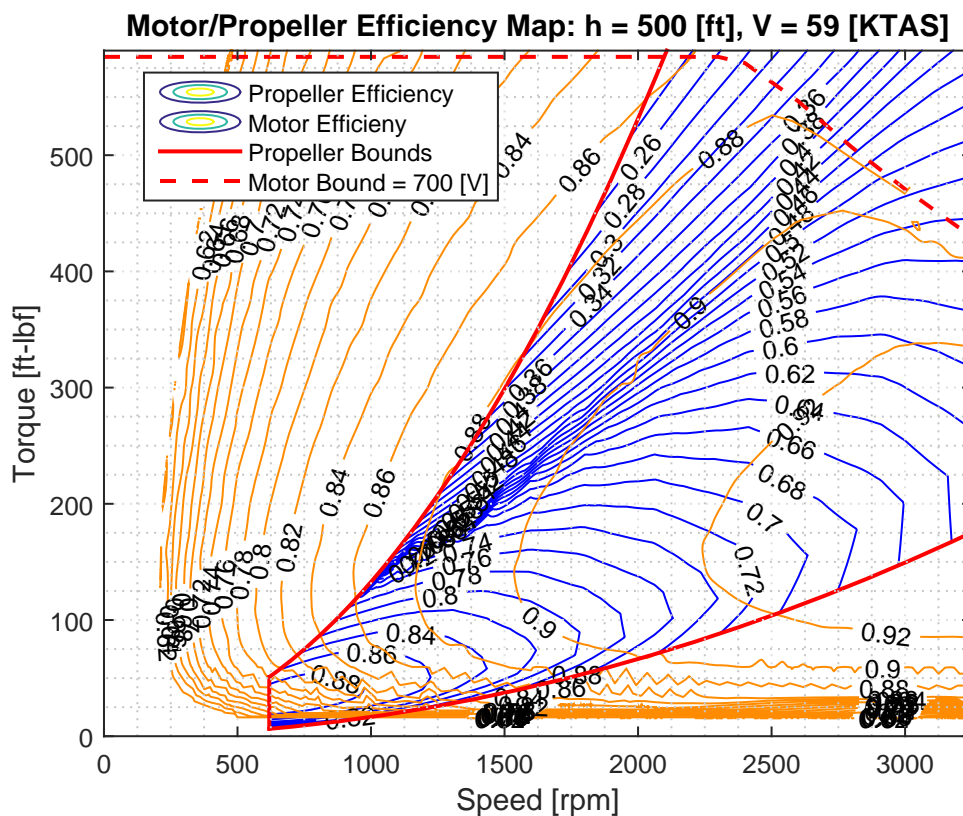


Figure 4.15. Electric motor and propeller efficiency overlay

The two contours are simply multiplied together to obtain the combined electric motor and propeller efficiency while taking both components limitations into account. Figure 4.16 displays the final net efficiency contour.

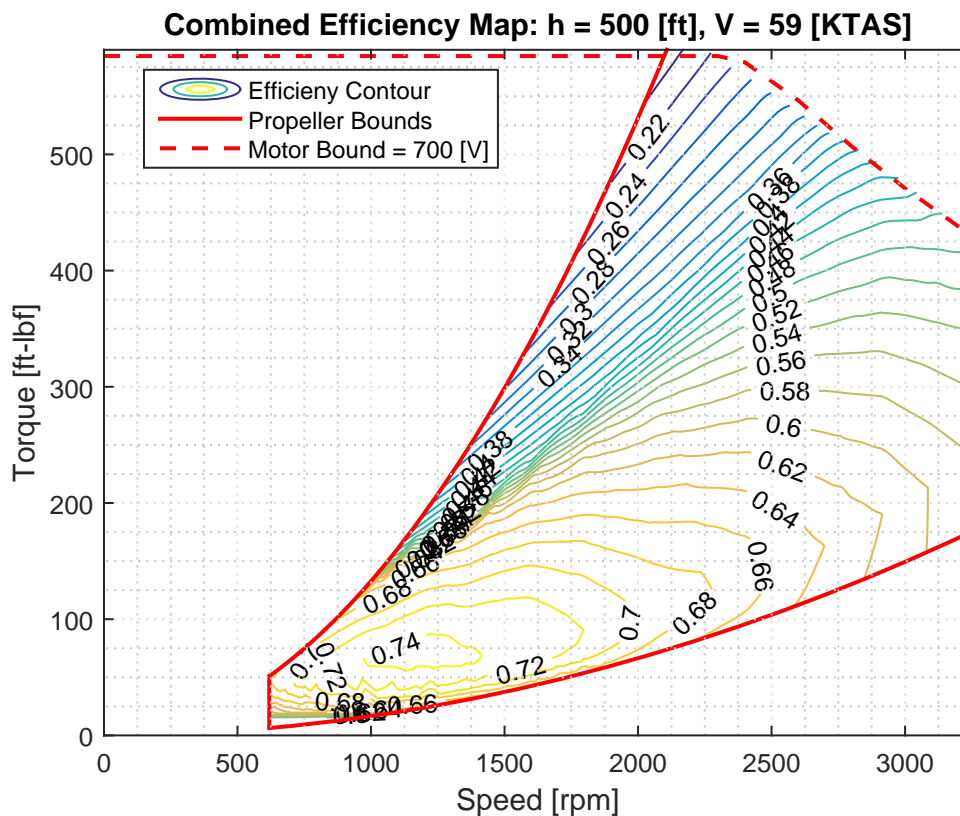


Figure 4.16. Electric motor and propeller combined efficiency map

Figure 4.16 shows that there appears to be a region of peak efficiency within the bounds for this electric motor and propeller combination. The final step is to now define how much thrust is being generated at this flight condition. A value of 500 lbf of thrust is assumed in this case even though it is not practical for the HK-36. This value of thrust will allow for further analysis in the following sections to better demonstrate the technology capability. Equation (3.31) is now used to compute torque for a constant thrust value across the RPM range on the efficiency map. The advantageous combination of an electric motor and controllable-pitch propeller are now shown in Figure 4.17.

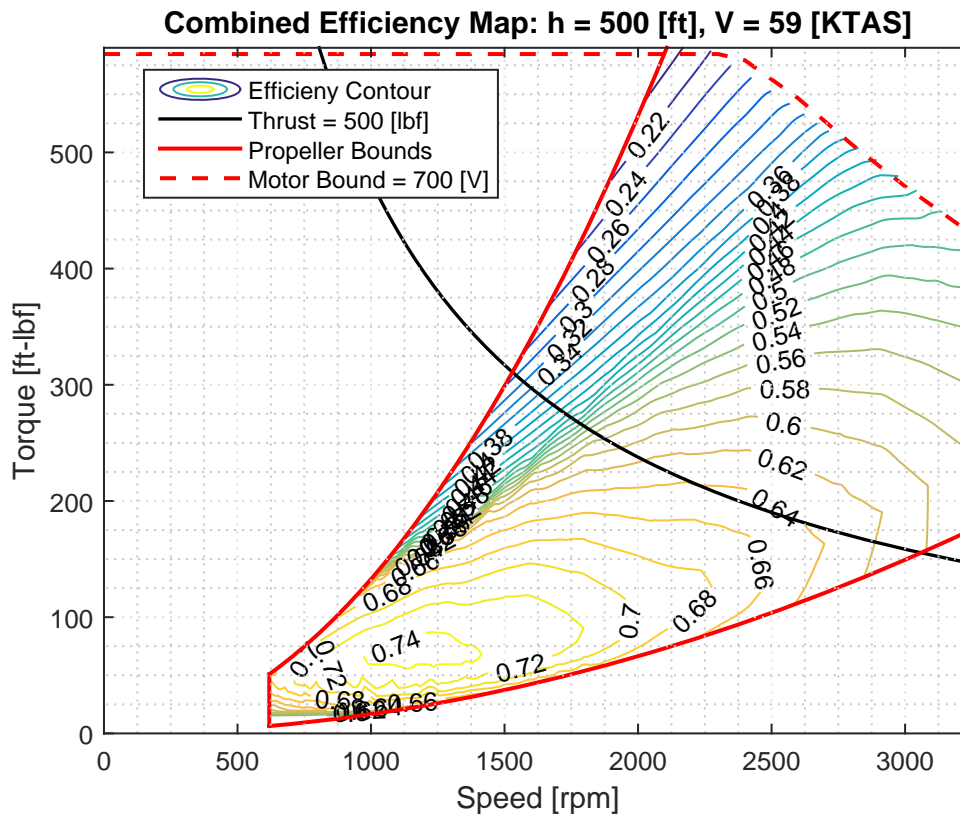


Figure 4.17. Combined efficiency with a constant thrust curve

The constant thrust curve shows that there are many different torque and RPM combinations that have a defined efficiency on both the electric motor and propeller. As a result of the electric motor's ability to vary torque and RPM independently, the coupling of a controllable-pitch propeller allows the pilot to pick and choose a torque and RPM to generate the given thrust. Unlike a gasoline engine, there are now multiple combinations of achieving the same thrust and therefore maintaining constant airspeed while having different solutions for efficiency. The electric motor in this case is viewed as the torque device, while the propeller is for speed control. When comparing operation to a traditional gasoline engine aircraft with a controllable-pitch propeller, the throttle here drives the torque of the electric motor while the propeller control drives the RPM. The key difference

is that the electric motor is not on a fixed speed, torque curve while a typical gasoline engine is so constrained.

4.3.4. Propeller Noise Mapping

Propeller noise is modeled using the Hamilton Standard methodology. Since one of the inputs to this method is power, noise can also be modeled at a given altitude and airspeed in a torque versus RPM grid by making use of Equation (3.24). The following inputs are used to generate the noise map shown in Figure 4.18 for the HK-36.

Table 4.3. Propeller and aircraft variable definitions for noise

Parameter	Variable	Value	Units
Aircraft velocity	V	59	KTAS
Altitude	h	500	ft
Ambient temperature	-	57.2	°F
Propeller diameter	D_p	6.04	ft
Number of propellers	n_p	1	-
Number of blades per propeller	n_b	2	-
Distance between aircraft and observer	d	500	ft
Azimuth angle	δ	90	deg
Propeller torque	Q	1 - 590	ft-lbf
Propeller RPM	RPM	1 - 3250	rpm

The ambient temperature is computed assuming standard atmosphere. The distance between the aircraft and observer as well as the azimuth angle have been arbitrarily chosen and will be updated later.

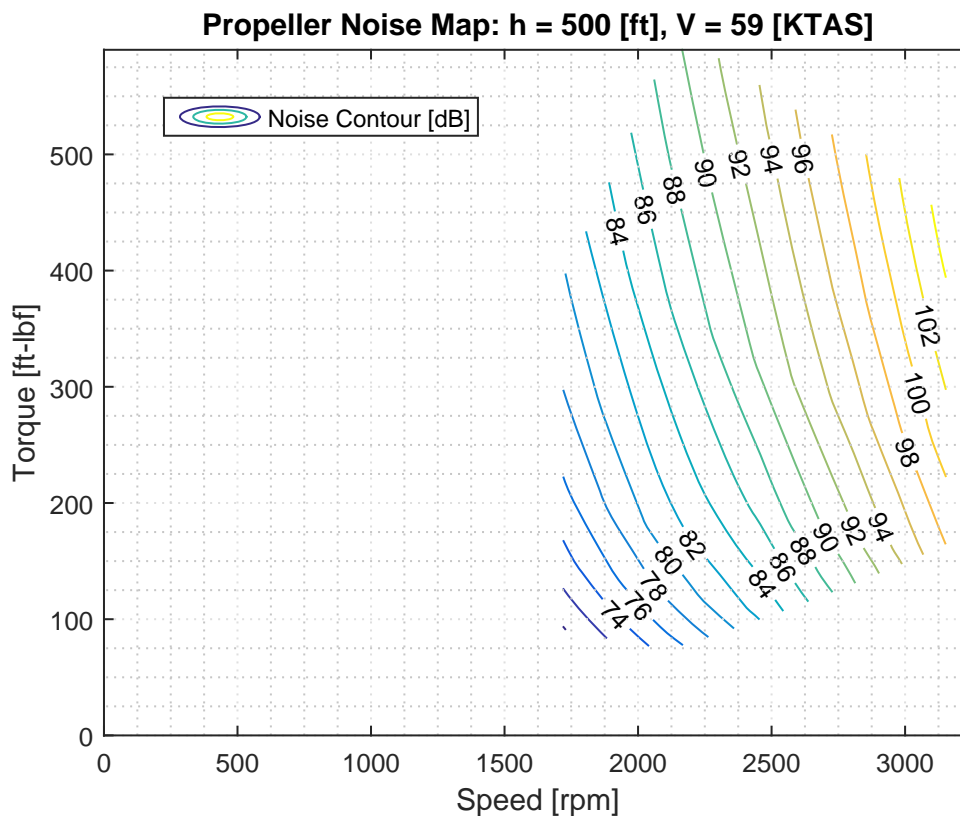


Figure 4.18. Propeller noise map

The propeller noise map shown in Figure 4.18 does not cover the majority of the plot due to the limitations of the methodology without allowing extrapolation. Nonetheless, this map can still be used as an additional overlay to the combined efficiency map shown in Figure 4.17. The map has also been preemptively cut to fit within the propeller and motor bounds where efficiency is defined. Figure 4.19 presents the combined efficiency and noise result.

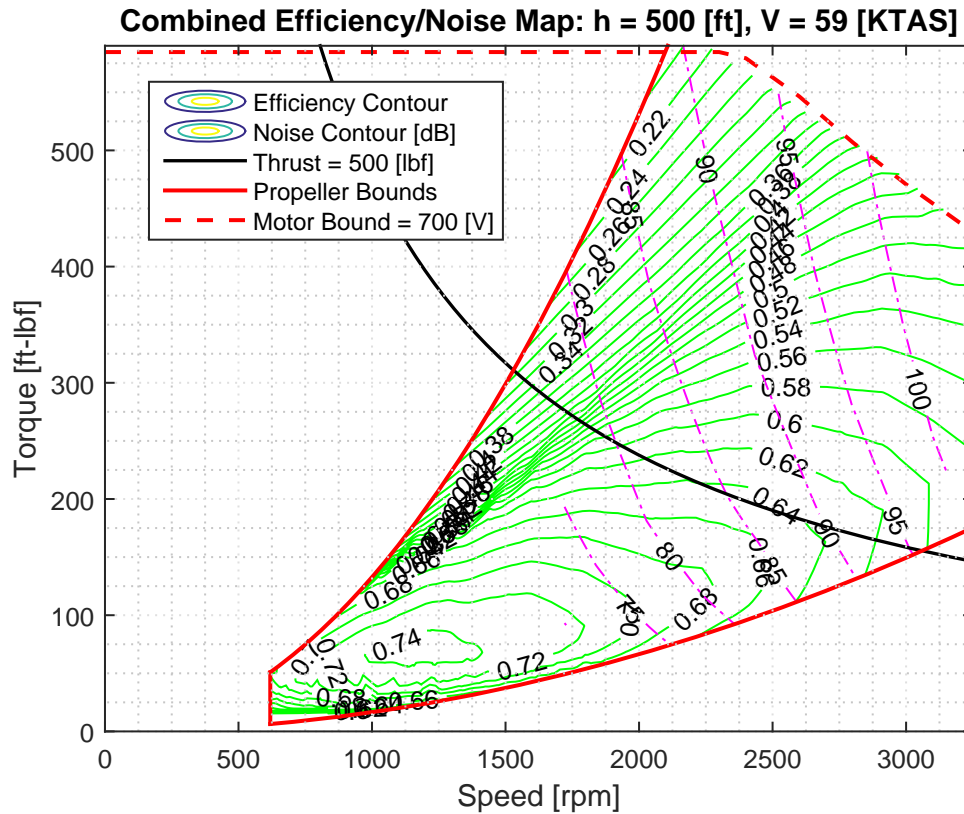


Figure 4.19. Combined efficiency and propeller noise

The efficiency contours of the combined electric motor and propeller are shown in green (solid contours) and the propeller noise contours are shown in magenta (long-short dashed contours). Figure 4.19 portrays a relationship that is unique to serial hybrid and fully electric aircraft. Recall that the pilot can pick and choose a torque and RPM to generate a given thrust. Prior to noise, the pilot would aim to optimize efficiency every time while maintaining constant thrust with no drawbacks. With propeller noise now a factor in this performance analysis, it is clear from Figure 4.19 that the peak efficiency comes at a cost of higher noise than other solutions. Figure 4.20 helps to further limit the range of operation at a given thrust by showing that an RPM faster than the maximum efficiency point does not offer any additional benefit.

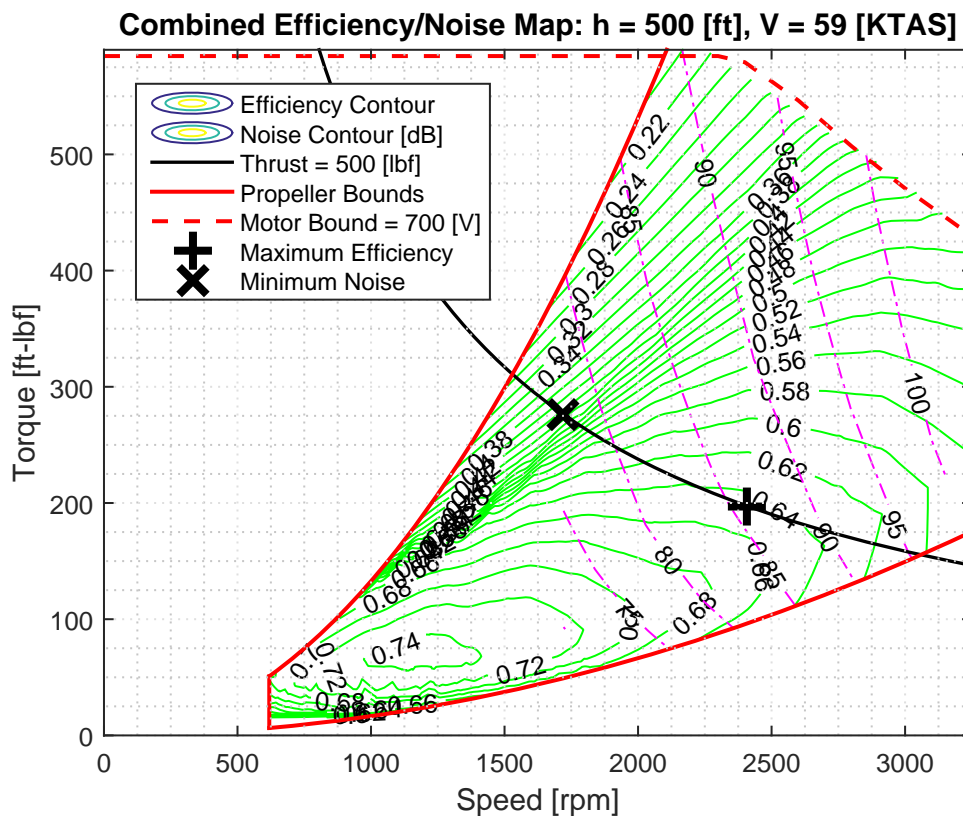


Figure 4.20. Location of maximum efficiency and minimum noise at constant thrust

The ideal range is operating between the minimum noise and maximum efficiency, where the trend in this case is that noise increases as efficiency increases up to the maximum efficiency point. Efficiency will then begin to decrease while noise continues to increase, rendering the high RPM region not practical for either efficiency or noise optimization. Remember that the noise contour is limited by the methodology and can possibly be expanded with other methods to encompass the full efficiency range. Ultimately, the choice now comes to flying efficiently, quietly, or somewhere in the middle.

4.3.5. Geographical Considerations for Propeller Noise Mitigation

The propeller contributes to the majority of noise in a serial hybrid aircraft. As previously mentioned, the pilot can reduce the noise at the cost of efficiency without changing airspeed. It is beneficial to apply this concept over a map to demonstrate the practical use of this noise mitigating technology. Due to the large amount of pilot training and aircraft operations, a map of the Daytona Beach, FL region shown in Figure 4.21 is used for reference.

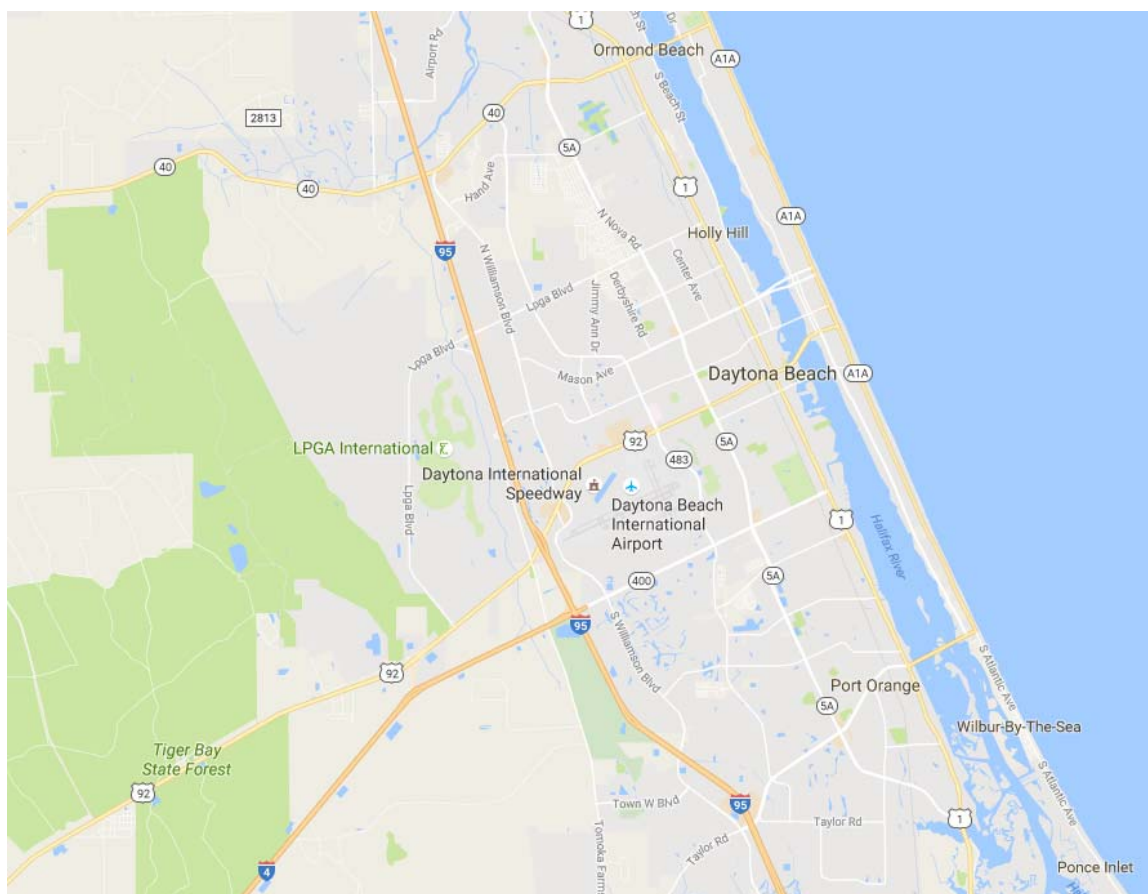


Figure 4.21. Map of the Daytona Beach, FL area

Recall the NSI where one (1) is the least sensitive and ten (10) is the most sensitive. This index can be applied over the surface of the Earth. Using the map in Figure 4.21, noise

sensitivity regions are arbitrarily drawn with applicable indices as demonstrated in Figure 4.22.

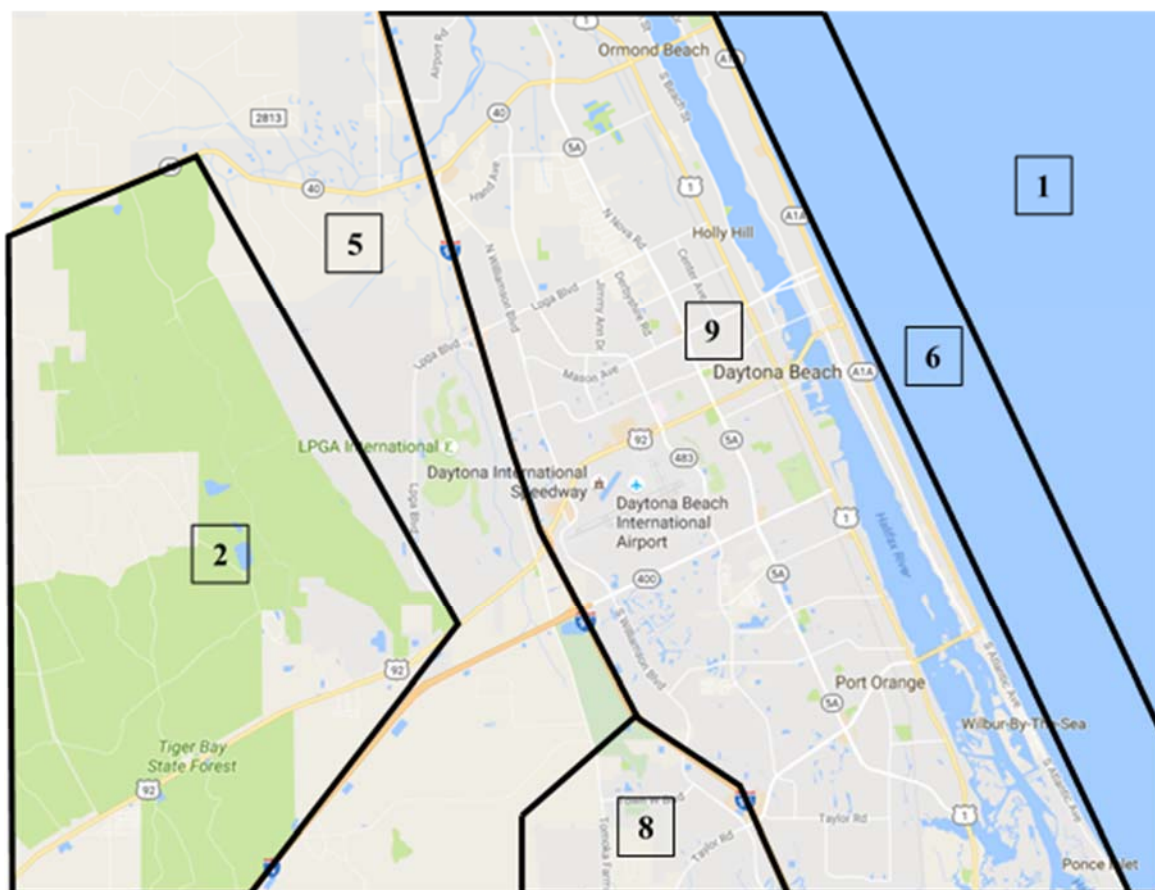


Figure 4.22. Noise sensitivity regions and applicable indices

With known sensitivity zones and corresponding indices, a pilot flying over the area would alter the propeller blade pitch to produce very little noise over the region with an index of nine (9) and can use any blade pitch while over the region with an index of one (1). This reduces noise over the primary populated area and includes transition zones so the pilot would begin to reduce noise when approaching the high sensitivity zones. The NSI concept can be applied to update Figure 4.20 and produce Figure 4.23.

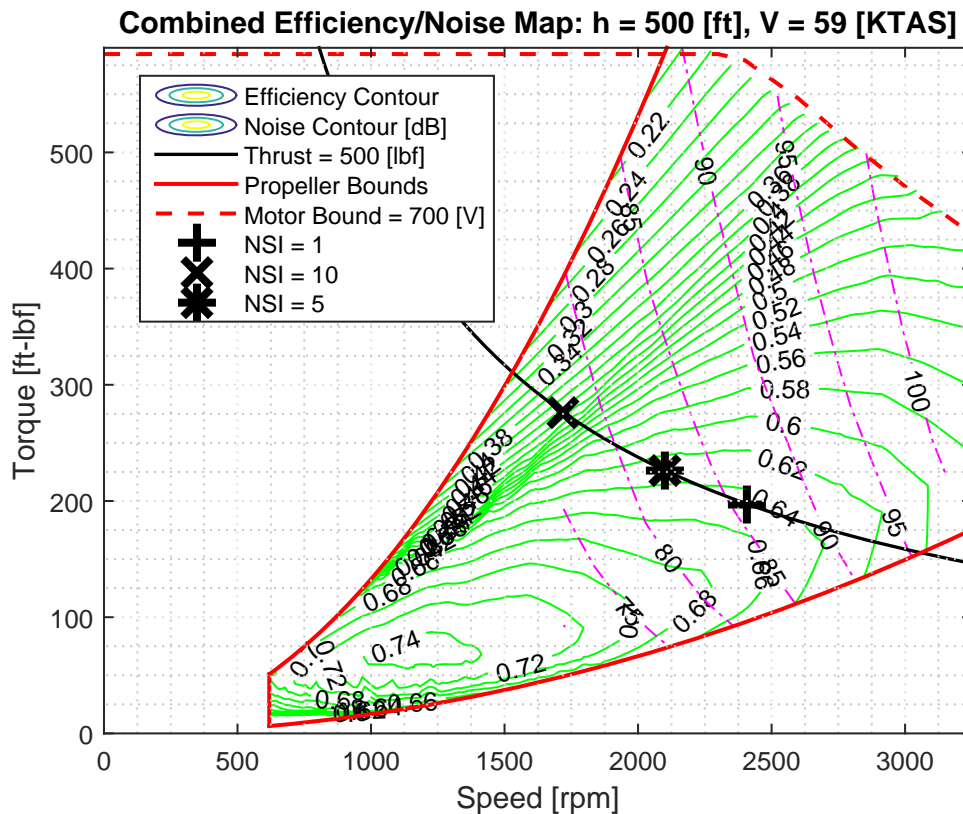


Figure 4.23. Location of various NSIs at constant thrust

The maximum efficiency and minimum noise points shown in Figure 4.20 are replaced by their corresponding NSIs of one (1) and ten (10) respectively. An additional NSI of five (5) is included to demonstrate that any arbitrary NSI can be selected to balance noise and efficiency based on geographical location.

Aircraft position and attitude now become a factor in generating the noise map shown in Figure 4.18. The procedure outlined in Section 3.6.2 is used to compute and update the distance and azimuth angle used in Table 4.3. The assumed position of the aircraft and observer are shown in Figure 4.24.

Table 4.4. Propeller and aircraft variable definitions for noise at a geographic location

Parameter		Variable	Value	Units
Aircraft velocity		V	59	KTAS
Ambient temperature		-	57.2	°F
Propeller diameter		D_p	6.04	ft
Number of propellers		n_p	1	-
Number of blades per propeller		n_b	2	-
Propeller torque		Q	1 - 590	ft-lbf
Propeller RPM		RPM	1 - 3250	rpm
Aircraft	Latitude	lat	29.185803	deg
	Longitude	lon	-81.045096	deg
	Pitch Angle	θ	10	deg
	Bank Angle	ϕ	0	deg
	Heading	ψ	70	deg
	Altitude	h	500	ft
Observer	Latitude	lat	29.186702	deg
	Longitude	lon	-81.042904	deg
	Altitude	h	32	ft



Figure 4.24. Geographical map of a Diamond HK-36 flyover

The marker located on the ground is the reference point for the observer (where the noise is measured). The latitude, longitude, and altitude above mean sea level are obtained using Google Earth. Note that Figure 4.24 is not drawn to scale nor is the HK-36 aircraft. Figure 4.24 serves to represent the analyzed condition. The aircraft is assumed to be departing Daytona Beach International Airport and is climbing. The analysis is conducted at a snapshot in time where the aircraft is flying at 59 KTAS at an altitude of 500 ft.

Once the distance and azimuth angle are computed based on the positions of the aircraft and observer, Table 4.3 is updated and a new noise map is developed.

Table 4.5. Propeller and aircraft variable definitions for noise

Parameter	Variable	Value	Units
Aircraft velocity	V	59	KTAS
Altitude	h	500	ft
Ambient temperature	-	57.2	°F
Propeller diameter	D_p	6.04	ft
Number of propellers	n_p	1	-
Number of blades per propeller	n_b	2	-
Distance between aircraft and observer	d	902.22	ft
Azimuth angle	δ	41.54	deg
Propeller torque	Q	1 - 590	ft-lbf
Propeller RPM	RPM	1 - 3250	rpm

The new noise map generated from the inputs in Table 4.5 will substitute into the noise map used in Figure 4.23 to create Figure 4.25. Referring to Figure 4.22 and Figure 4.24, the aircraft is currently located in a zone with an NSI of nine (9).

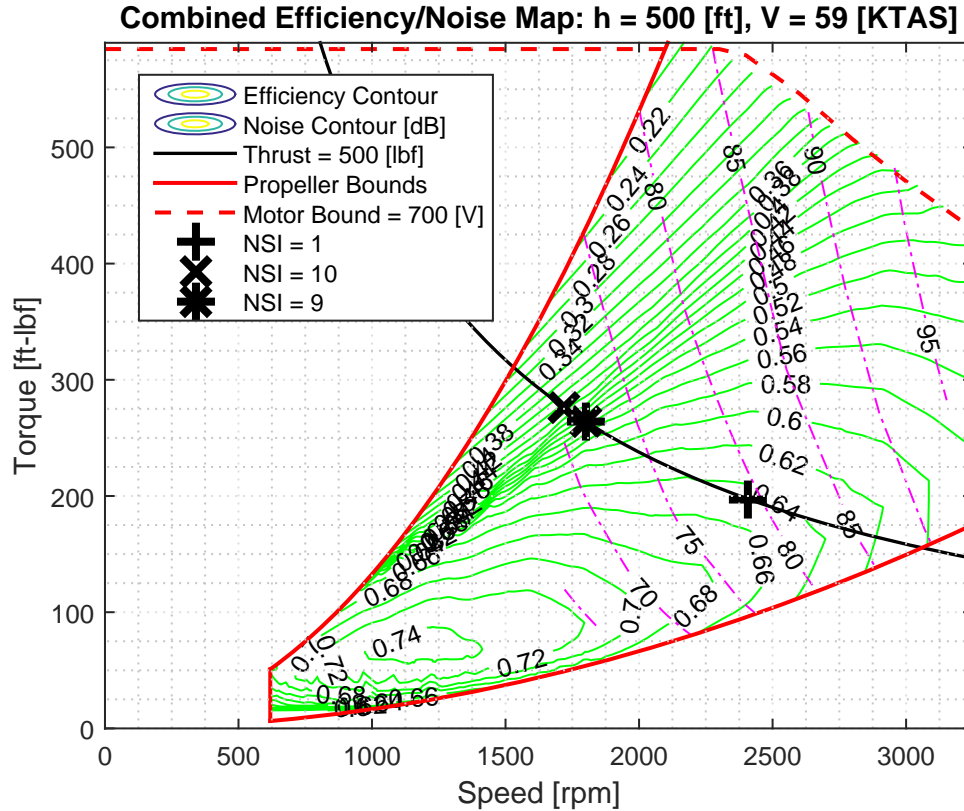


Figure 4.25. Efficiency and noise given aircraft and observer position

The noise mitigation concept applies regardless of the thrust value used. The following table summarizes the results displayed in Figure 4.25.

Table 4.6. Diamond HK-36 noise and efficiency results

Parameter	NSI = 1	NSI = 9	NSI = 10	Units
Propeller rotational speed	2410	1798	1722	rpm
Propeller torque	197	264	276	ft-lbf
Propeller noise	79.3	71.9	70.8	dB
Combined efficiency	0.647	0.518	0.430	-
Thrust	500	500	500	lbf

The noise measured can range between 79.3 dB and 70.8 dB depending on the propeller pitch setting. The various propeller settings are achievable at a given altitude and airspeed

due to the electric motor and controllable-pitch propeller combination. The current NSI requires the pilot to set the propeller so that less noise is produced at the cost of efficiency. Once the aircraft flies into a lower sensitivity zone, the pilot can readjust the propeller blade angle to produce more noise while improving net efficiency.

4.4. Flight Envelope Overlay

Recall the Diamond HK-36 flight envelope as shown in Figure 4.5 (repeated below in Figure 4.26) and how the propeller and motor efficiency were assumed to be equal to one (1).

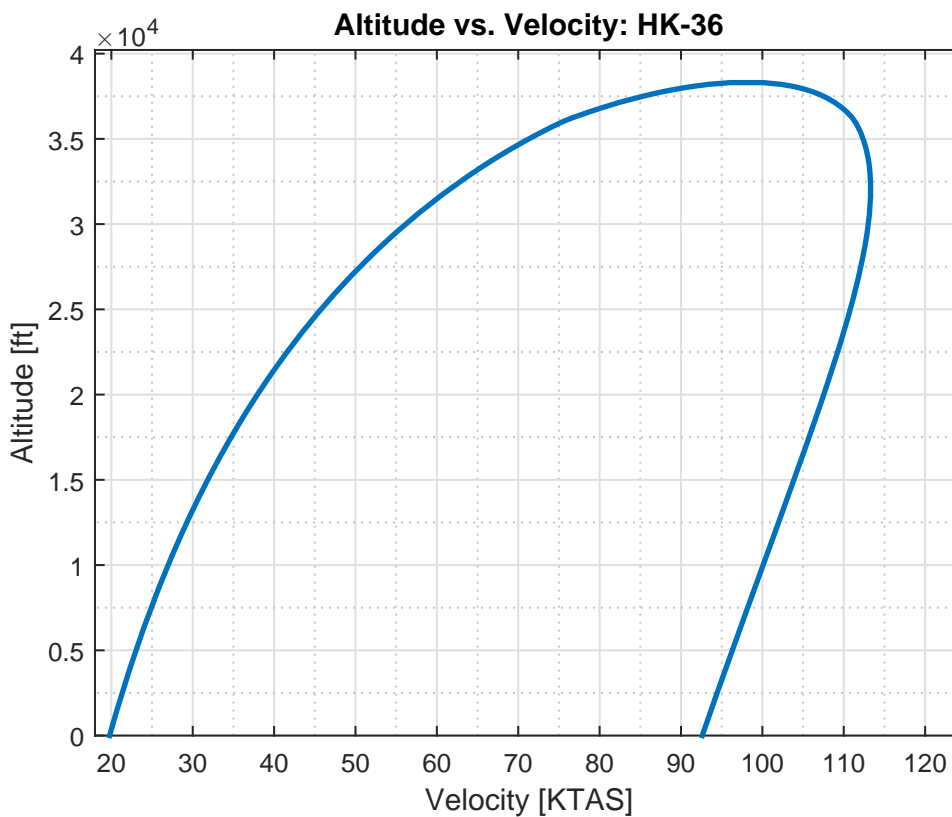


Figure 4.26. Diamond HK-36 100% hybrid flight envelope

Efficiency and noise can be added to this flight envelope using the results from Sections 4.3.3, 4.3.4, and 4.3.5. These sections show that for a given altitude and airspeed, an efficiency and noise map can be generated. This map can be regenerated across altitudes and airspeeds within the flight envelope to create an efficiency and noise overlay. Since there are many choices for efficiency and associated noise at a given thrust value, for analysis purposes, it is assumed that the pilot is maximizing efficiency ($NSI = 1$) and accepting the resulting noise at the maximum efficiency. This analysis will assume the same YASA-750 electric motor and MT-Propeller are used.

4.4.1. Efficiency

The flight envelope uses the assumption that the aircraft is in steady, level flight. To determine the required thrust at a given altitude and airspeed, it is assumed that thrust is equal to drag. The denominator of Equation (3.16) is used to compute the drag and therefore required thrust for the HK-36. For every altitude and airspeed in the flight envelope shown in Figure 4.26, the computed thrust required is plotted on the efficiency and noise map and the maximum efficiency is extracted, saved, and ultimately plotted onto the flight envelope as shown in Figure 4.27.

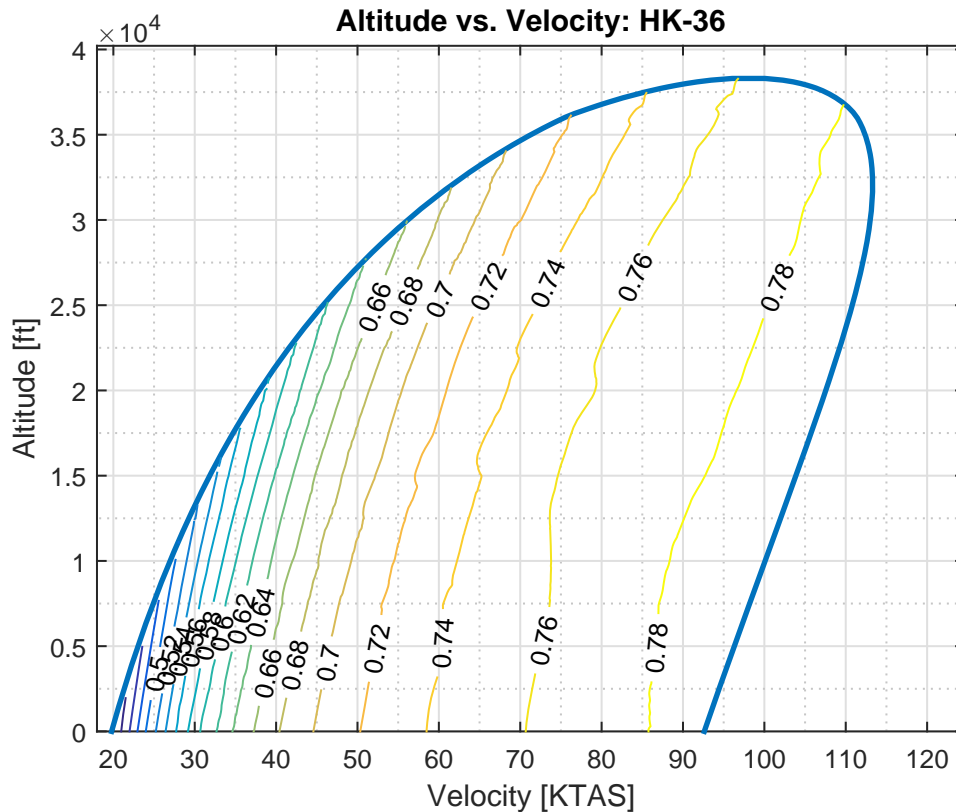


Figure 4.27. Diamond HK-36 flight envelope maximum efficiency

The best combined electric motor and propeller efficiencies occur at faster airspeeds based on Figure 4.27. It is easily noticed that the efficiency gain towards the faster end of the flight envelope is not nearly as significant as the slower end. It is important to keep in mind that the faster airspeeds, while more energy efficient, also use available energy quicker.

4.4.2. Noise

The HK-36 flight envelope does not produce a consistent noise contour due to the low power required in cruising flight. As a result, the thrust curve across the efficiency and noise map only intersects the noise map at a select few airspeeds and altitudes and is not practical as a flight envelope overlay.

Many different aircraft can create a complete noise contour within the flight envelope, however, this is not the most practical approach to analyze noise. In cruising flight, power is reduced from the takeoff or climb configuration and the aircraft is often cruising at an altitude that produces very little measurable noise on the ground due to the distance the noise must travel. While a low altitude cruise power is still audible, it would only cover a small portion of the entire flight envelope.

5. Conclusion

5.1. Significant Results

Serial hybrid electric aircraft allow the expansion of a fully electric aircraft's flight envelope with the ability to maximize efficiency and mitigate noise. The blending of battery and gas specific energies expands the envelope significantly even when only a small percentage of the energy weight fraction is contributed to gas. Battery specific energy improvements alone expand the flight envelope. The advantage of using battery technology is that batteries continuously get better on an energy basis whereas fuel does not. Over time, the hybridization of the aircraft can move closer towards fully electric while maintaining the same flight envelope as a hybrid aircraft. Present day fully electric aircraft require hybridization to achieve the performance goals that gasoline aircraft can offer.

The serial hybrid configuration allows for a unique exploit of combining an electric motor and controllable-pitch propeller. By the nature of the configuration, the propeller is turned by the electric motor alone. As long as the electric motor has an appropriate motor controller, torque and RPM can be varied independently to be able to generate constant thrust at a variety of torque and RPM combinations, each with a different efficiency and noise output. This allows the pilot to operate either more quietly or more efficiently, depending on their geographical location and the noise sensitivity of the area.

5.2. Future Work

The flight envelope is developed based on a parabolic drag model and does not account for altitude effects on air breathing components, stall speed, structural limitations, human physiology, or air traffic control concerns. All of these assumptions can be removed

and other flight envelope limitations not accounted for or mentioned can be included as well.

The electric motor and propeller data were manufacturer provided for only one type of motor and propeller. Follow up work to this would be to either use other electric motors and propellers or to be able to generate a way of computing new efficiency tables. The electric motor would need a physics based model to be developed to generate new efficiency maps. The propeller can use methods such as blade element theory to be able to define a custom propeller geometry and develop an efficiency lookup table.

The Hamilton Standard noise model is the only one used here for analysis. Other propeller noise models may yield different results and can expand the range of which the results are valid to encompass a larger portion of the efficiency map.

Noise sensitive airspace can also be better defined over the surface of the Earth. The NSI of a region can be derived based on population, proximity to national parks, or other geographical landmarks. The index can also change dynamically based on the time of day or the day itself.

REFERENCES

- ATAG. (2010). *Beginner's Guide to Aviation Efficiency*. Air Transport Action Group.
- ATAG. (2016, December 23). *Facts and Figures*. Retrieved from <http://www.atag.org/facts-and-figures.html>
- Boca Raton Airport. (2016, December 23). Retrieved from <http://bocaairport.com/noise-abatement/procedures/>
- CAEP. (2010). Committee on Aviation Environmental Protection (CAEP) Eighth Meeting., (p. Agenda Item 2). Montreal.
- Clarke, S. (2015). LEAPTech HEIST Power Architecture and Testing. *2015 AIAA Aviation Technology, Integration, and Operations Conference*. Dallas: NASA.
- Clarke, S. (2016). SCEPTOR Power System Design: Experimental Electric Propulsion System Design and Qualification for Crewed Flight Testing. *AIAA Aviation Technology, Integration, and Operations Conference*. Washington D.C.: NASA.
- Costello, L. A. (2011). *State of the Art of Piloted Electric Airplanes, NASA's Centennial Challenge Data and Fundamental Design Implications*. Daytona Beach: Embry-Riddle Aeronautical University.
- FAA. (2016). *FAA Aerospace Forecast Fiscal Years 2016-2036*.
- Fehrenbacher, J. (2011). *Electric Motor & Power Source Selection for Small Aircraft Propulsion*. West Lafayette: College of Technology Directed Projects.
- GAMA. (2014). *General Aviation Statistical Databook & 2015 Industry Outlook*.
- Gleyzer, A. (2017, January 15). Retrieved from Computing Distances: <http://www.cs.nyu.edu/visual/home/proj/tiger/gisfaq.html>
- Gudmundsson, S. (2014). *General Aviation Aircraft Design: Applied Methods and Procedures*. New York: Elsevier Inc.
- Hepperle, M. (2012). *Electric Flight - Potential and Limitations*. Braunschweig: German Aerospace Center.
- ICAO. (2016, December 23). *Noise Abatement Operational Procedures*. Retrieved from ICAO Environment: <http://www.icao.int/environmental-protection/Pages/Noise-Abatement-Operational-Procedures.aspx>
- Marwa, M. (2016). *Analytic and Numeric Forms of Range and Endurance for Hybrid and Electric Aircraft*. Daytona Beach: Embry-Riddle Aeronautical University.
- SAE. (1977). *Prediction Procedure for Near-Field and Far-Field Propeller Noise*. Warrendale: Society of Automotive Engineers Inc.
- Santa Monica Municipal Airport. (2016, December 23). Retrieved from <http://www.smgov.net/departments/airport/content.aspx?id=9006>
- U.S. Department of Energy. (2016, December 23). *The eGallon*. Retrieved from U.S. Department of Energy: <https://energy.gov/articles/egallon-how-much-cheaper-it-drive-electricity>

